Human Brain Project
Education Programme

5th HBP STUDENT CONFERENCE ON INTERDISCIPLINARY BRAIN RESEARCH

1–4 FEBRUARY 2021
VIRTUAL EVENT

BOOK OF ABSTRACTS

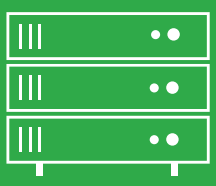

A Dynamical Model of Action Selection and Dopamine Related Movement Disorders

Ayça Kepçe1*, Neslihan Serap Şengör2

[1] Neuroscience Modelling and Research Group, Istanbul Technical University, Istanbul, Turkey
[2] Department of Electrical and Computer Engineering, Technical University Munich, Munich, Germany
*ayca.kepce@tum.de

INTRODUCTION

The action selection mechanism in humans is maintained in the loop of basal ganglia-cortex-thalamus [1,2]. This loop is mainly regulated by the neurotransmitter dopamine, which is found in dopaminergic corticostriatal neurons [3,4]. Abnormal levels of dopamine are related to movement disorders. Parkinson's disease and Huntington's disease are related to lack and excess of dopamine, respectively [5,6,7].

This study proposes an action selection model with dynamical approach, which is capable of choosing between different actions, depending on the initial conditions, dopamine levels, and stimuli. Further, by controlling the dopamine parameter, we obtain hypokinesia and hyperkinesia seen in Parkinson's and Huntington's diseases.

METHODS

The direct and indirect pathways in the cortex-basal ganglia-thalamus loop [4,7] are expressed with continuous nonlinear differential equations and activation functions, which are given below. There are two different actions (also called "channels") defined with six variables, p_i (cortex), m_i (thalamus), r_i (striatum), e_i (globus pallidus externus), n_i (subthalamic nuclei), and u_i (globus pallidus internus/substantia nigra pars reticula). The index of the variables, i denote the channel number, where $i \in \{1,2\}$.

$$\begin{bmatrix}\dot{p_1}(t)\\ \dot{p_2}(t)\end{bmatrix} = -\begin{bmatrix}\lambda_{p1} & \lambda_{p2}\end{bmatrix}\begin{bmatrix}p_1(t)\\ p_2(t)\end{bmatrix} + \begin{bmatrix}W_{mp1} & 0\\ 0 & W_{mp2}\end{bmatrix}\begin{bmatrix}f(m_1(t))\\ f(m_2(t))\end{bmatrix} + \begin{bmatrix}a_1\\ a_2\end{bmatrix}$$

$$\begin{bmatrix}\dot{m_1}(t)\\ \dot{m_2}(t)\end{bmatrix} = -\begin{bmatrix}\lambda_{m1} & \lambda_{m2}\end{bmatrix}\begin{bmatrix}m_1(t)\\ m_2(t)\end{bmatrix} + \begin{bmatrix}W_{pm1} & 0\\ 0 & W_{pm2}\end{bmatrix}\begin{bmatrix}f(p_1(t))\\ f(p_2(t))\end{bmatrix} - \begin{bmatrix}W_{um1} & 0\\ 0 & W_{um2}\end{bmatrix}\begin{bmatrix}f(u_1(t))\\ f(u_2(t))\end{bmatrix}$$

$$\begin{bmatrix}\dot{r_1}(t)\\ \dot{r_2}(t)\end{bmatrix} = -\begin{bmatrix}\lambda_{r1} & \lambda_{r2}\end{bmatrix}\begin{bmatrix}r_1(t)\\ r_2(t)\end{bmatrix} + \begin{bmatrix}W_{pr1} & 0\\ 0 & W_{pr2}\end{bmatrix}\begin{bmatrix}h(p_1(t))\\ h(p_2(t))\end{bmatrix}$$

$$\begin{bmatrix}\dot{e_1}(t)\\ \dot{e_{2(t)}}\end{bmatrix} = -\begin{bmatrix}\lambda_{e1} & \lambda_{e2}\end{bmatrix}\begin{bmatrix}e_1(t)\\ e_2(t)\end{bmatrix} - \begin{bmatrix}W_{re1} & 0\\ 0 & W_{re2}\end{bmatrix}\begin{bmatrix}f(r_1(t))\\ f(r_2(t))\end{bmatrix} + \begin{bmatrix}W_{ne1} & 0\\ 0 & W_{ne2}\end{bmatrix}\begin{bmatrix}f(n_1(t))\\ f(n_2(t))\end{bmatrix}$$

$$\begin{bmatrix}\dot{n_1}(t)\\ \dot{n_2}(t)\end{bmatrix} = -\begin{bmatrix}\lambda_{n1} & \lambda_{n2}\end{bmatrix}\begin{bmatrix}n_1(t)\\ n_2(t)\end{bmatrix} - \begin{bmatrix}W_{en1} & 0\\ 0 & W_{en2}\end{bmatrix}\begin{bmatrix}f(e_1(t))\\ f(e_2(t))\end{bmatrix} + \begin{bmatrix}W_{pn1} & 0\\ 0 & W_{pn2}\end{bmatrix}\begin{bmatrix}f(p_1(t))\\ f(p_2(t))\end{bmatrix}$$

$$\begin{bmatrix}\dot{u_1}(t)\\ \dot{u_2}(t)\end{bmatrix} = -\begin{bmatrix}\lambda_{u1} & \lambda_{u2}\end{bmatrix}\begin{bmatrix}u_1(t)\\ u_2(t)\end{bmatrix} - \begin{bmatrix}W_{ru1} & 0\\ 0 & W_{ru2}\end{bmatrix}\begin{bmatrix}f(r_1(t))\\ f(r_2(t))\end{bmatrix} - \begin{bmatrix}W_{eu1} & 0\\ 0 & W_{eu2}\end{bmatrix}\begin{bmatrix}f(e_1(t))\\ f(e_2(t))\end{bmatrix} + \begin{bmatrix}W_{nu11} & W_{nu21}\\ W_{nu12} & W_{nu22}\end{bmatrix}\begin{bmatrix}f(n_1(t))\\ f(n_2(t))\end{bmatrix}$$

$$f(x) = 1/(1 + e^{-3x+0.8})$$

$$h(x) = f(x - (1 - \theta))$$

The connections are expressed with W_{ijk} (from i to j, k designating the channel number), the stimulus and dopamine parameter are denoted with a_k (k is the channel number) and θ,

respectively. The stimuli a can be a visual cue about a certain behavior, e.g. seeing an apple is a stimulus for the action of grabbing the apple. The dopamine parameter θ is expressed on the cortex-striatum connection via the activation function $\mathrm{h(x)}$. The initial conditions can be considered of the current intrinsic state of the person about that action, e.g. being hungry for the grabbing the apple example. The values of the parameters given in Table 1 are determined in our previous work [7,8] and tuned for this model throughout the analyses.

Table 1: Values of the parameters

Symbol	Value
$W_{um1,2}, W_{ru1,2}, W_{pr1,2}, W_{pn1,2}$	1
$W_{re1,2}, W_{en1,2}, W_{pm1,2}, W_{ne1,2}$	0.5
$W_{mp1,2}$	1.5
$W_{nu1,2}$	0.725
$\lambda_{p1,2}, \lambda_{m1,2}$	0.5
$\lambda_{r1,2}, \lambda_{e1,2}, \lambda_{n1,2}, \lambda_{u1,2}$	1
θ	$\in$ [0.1,0.95]
$a_{1,2}$	$\in$ [0.1,0.15]

There are four scenarios of the model's decision: selecting no action, the first action, the second action, or both actions. The decision is one of these scenarios, depending on the initial conditions, stimuli, and dopamine. If initially $p_1 > p_2$, then the first channel has a head start. When stimulus to the first channel is greater, the model "has more reasons" to choose that action. On the other hand, dopamine equally affects both channels.

RESULTS

In order to determine the parameters, several dynamical analyses are conducted: time, bifurcation, and domain of attraction analyses. The stimuli and the initial conditions would vary depending on the environment. Therefore, we analyzed the behavior of the model under different values of stimuli and initial conditions. Further, different values of dopamine parameter are investigated to model movement disorders.

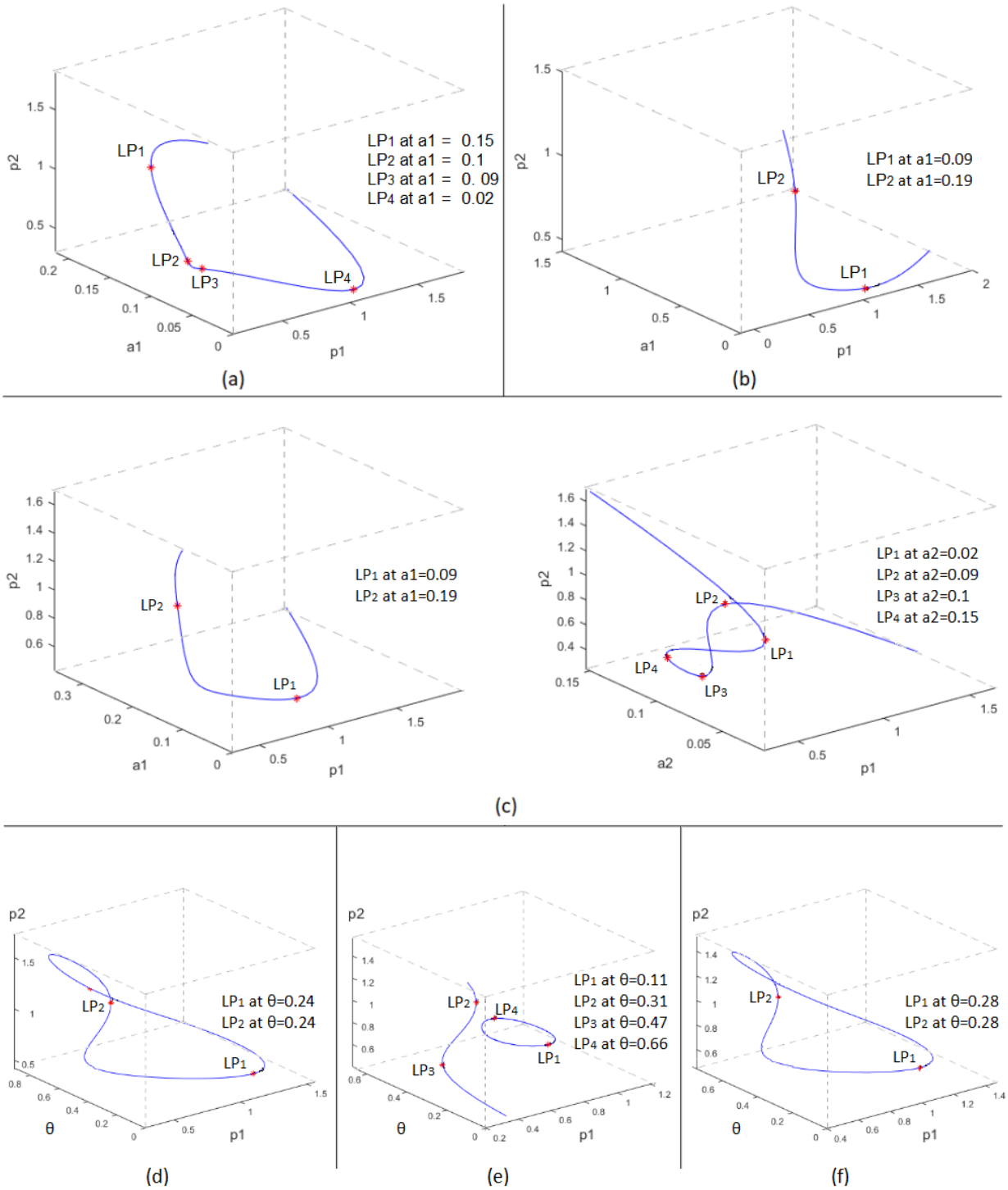

Figure 1: Bifurcation graphs of a and θ. LP denotes saddle-node bifurcation. For $\theta = 0.5$, bifurcation analysis of a_1 when a) $a = [0.1; 0.1]$ and b) $a = [0.15; 0.15]$. For $\theta = 0.5$, bifurcation analysis of a_1 and a_2 when $a = [0.1; 0.15]$. Bifurcation analyses of θ, when d) $a = [0.1;\ 0.1]$, e) $a = [0.1; 0.15]$ and f) $a = [0.15; 0.15]$.

The bifurcation analyses of a for different stimuli are given in Figure 1(a)-(c). The bifurcation analyses of a for different θ values are also investigated, no bifurcation points occurred in the range of $[0.1, 0.15]$. Then the bifurcation graphs of θ are obtained as given in Figure 1(d) to 1(f). The results of the case $a = [0.15; 0.1]$ is symmetrical with $a = [0.1; 0.15]$.

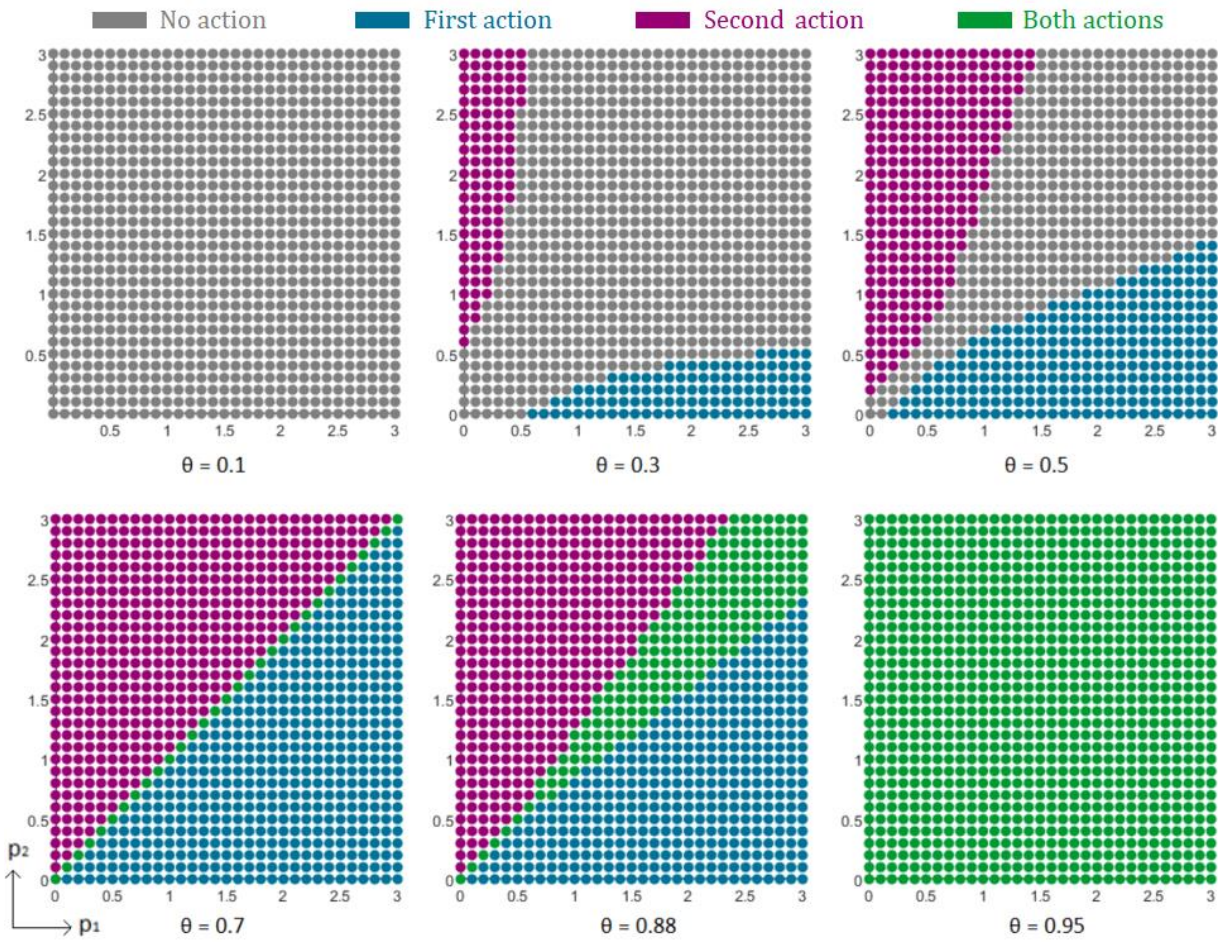

Figure 2: The domain of attraction graphs for $a = [0.1; 0.1]$ and different values of θ.

The domain of attraction graphs for different a and θ values are obtained, as the one given in Figure 2. The initial values of the cortex variable of the first and second channels are located on x and y axes, respectively. Each dot represents the result of the time analysis at given initial conditions. The i^{th} action is considered to be chosen, if $p_i \geq 1$. The green (grey) dots represent both (no) actions are chosen and the blue (purple) dots represent the first (second) action is chosen.

The graphs in Figure 2 are obtained when $a = [0.1,0.1]$. For $\theta = 0.1$ the model chooses no actions, regardless of the initial conditions. Both actions are chosen for every initial condition when $\theta = 0.95$. For the intermediate values of θ, the model chooses the action with the greater initial value of cortex variable. If the initial values of both channels are close to each other, then the model chooses no action or both of the actions, depending on the θ value.

For the cases that the i^{th} stimulus is greater than the other, the i^{th} action is chosen for the intermediate values of θ. No action Is chosen at any of the initial conditions when $\theta = 0.1$ and both actions are chosen at every initial condition when $\theta = 0.95$.

DISCUSSION

We proposed a dynamical model that selects actions between two choices depending on the initial conditions and the stimuli. The model should show a stable behavior as the stimuli change. Therefore, the range of the stimuli is chosen as $a \in [0.1, 0.15]$, avoiding all of the bifurcation points.

Since we wanted to replicate the hypokinetic and hyperkinetic states as θ changes, the behavior of the model should change quantitatively. Therefore, the range of dopamine parameter should contain at least one saddle-node bifurcation. Considering the bifurcation graphs given in Figure 1(d)-(f), the range is chosen as $\theta \in [0.1, 0.95]$. For $\theta = 0.1$ and $\theta = 0.95$, the hypokinesia in Parkinson's and the hyperkinesia in Huntington's are obtained, respectively. For the intermediate values of θ, the model behaves as a healthy person who evaluates the situation based on the stimuli and initial conditions, and decides accordingly.

There are some deep brain stimulation (DBS) applications for treating the symptoms of these conditions [9,10]. We believe that our humble model can give intuition for developing more efficient DBS models for treating these diseases. Moreover, the model can be realized on a hardware, e.g. FPGA or a robot microcontroller, due to its simplicity.

REFERENCES

[1] Friend, D.M. & Kravitz, A.V., 2014. Working together: basal ganglia pathways in action selection. *Trends in neurosciences*, 37(6), pp.301-303.

[2] Kropotov, J.D. & Etlinger, S.C., 1999. Selection of actions in the basal ganglia–thalamocortical circuits: Review and model. *International Journal of Psychophysiology*, 31(3), pp.197-217.

[3] Ferré, S., Fuxe, K., Fredholm, B. B., Morelli, M., & Popoli, P. (1997). Adenosine–dopamine receptor–receptor interactions as an integrative mechanism in the basal ganglia. *Trends in neurosciences*, 20(10), 482-487.

[4] Elibol, R., & ¸Sengör, N. S. (2015, October). A computational model of basal ganglia circuits investigating the role of dopamine on direct and indirect pathways. *In 2015 Medical Technologies National Conference (TIPTEKNO)* (pp. 1-4). IEEE.

[5] Scatton, B., Rouquier, L., Javoy-Agid, F., & Agid, Y. (1982). Dopamine deficiency in the cerebral cortex in Parkinson disease. *Neurology,* 32(9),1039-1039.

[6] Jahanshahi, A., Vlamings, R., Kaya, A. H., Lim, L. W., Janssen, M.L., Tan, S., ...& Temel, Y. (2010). Hyperdopaminergic status in experimental Huntington disease. J*ournal of Neuropathology & Experimental Neurology*, 69(9), 910-917.

[7] Kepce, A., Iris, S., ¸Sengor, N. S. (2020, April). A Neural Network Model for the Role of Dopamine on Action Initiation and Its Realization on FPGA. *In 28th IEEE Conference on Signal Processing and Communications Applications (SIU)*. IEEE.

[8] Kepce, A., &¸Sengor, N. S. (2019, October). Bifurcation Analysis of A Mass Model Related to Cortex-Basal Ganglia-Thalamus Loop. *In 2019 Medical Technologies Congress (TIPTEKNO).* IEEE.

[9] Little, S., Pogosyan, A., Neal, S., Zavala, B., Zrinzo, L., Hariz, M., ... & Green, A. L. (2013). Adaptive deep brain stimulation in advanced Parkinson disease. *Annals of neurology*, *74*(3), 449-457.

[10] Wojtecki, L., Groiss, S. J., Hartmann, C. J., Elben, S., Omlor, S., Schnitzler, A., & Vesper, J. (2016). Deep brain stimulation in Huntington's disease—preliminary evidence on pathophysiology, efficacy and safety. *Brain sciences*, *6*(3), 38.

Highway to a biologically-grounded neural field model of cerebellum

Roberta Maria Lorenzi[1*], Alice Geminiani[1], Claudia A.M. Gandini Wheeler-Kingshott[1,2,3], Fulvia Palesi[1], Claudia Casellato[1], Egidio D'Angelo[1]

[1] Department of Brain and Behavioral Sciences, University of Pavia, Via Forlanini 6, Pavia, Italy
[2] Queen Square MS Centre, Department of Neuroinflammation, UCL Institute of Neurology, Russell Square House, Russell Square, WC1B 5EH, London, United Kingdom
[3] IRCCS Mondino Foundation, Via Mondino 2, Pavia, Italy

*robertamaria.lorenzi01@universitadipavia.it

INTRODUCTION

The brain is made of interconnected networks generating its global activity. Several modelling approaches are used to investigate the contribution of local networks to brain global dynamics. While biophysically detailed implementations allow to distinguish the contribution of single neurons to brain dynamics, they are usually too complex for large-scale simulations and need to be condensed into simpler and more abstract models. Typically, these take the form of neural masses or mean fields, which oversimply the physiological properties of an entire neuronal circuit [1,2,3]. What we propose here is an advanced mean field model of the cerebellar cortex that maintains a fundamental set of physiological and structural properties of this specific circuit.

While the cerebellum contains about 50% of all brain neurons, is deeply interconnected with the rest of the brain and remarkably contributes to generate ensemble brain dynamics [4] , the mean field models developed so far are tailored to the cerebral cortex only but may not be effective to capture cerebellar cortex properties. Indeed, the cerebellar circuit organization is peculiar and markedly differs from that of the cerebral cortex. A mean field model of the cerebellar circuit should therefore consider its complex neuronal features, multi-layer organization, quasi-crystalline geometry and local connectivity.

This work aims to develop a mean field model retaining the salient properties of the cerebellar circuit. The model will be used not just to provide theoretical insight on cerebellar network functioning but also to simulate the impact of cerebro-cerebellar interactions on whole brain dynamics in the framework of The Virtual Brain (TVB).

METHODS

The design of the cerebellar mean-filed model starts from an accurate and extensive knowledge of cerebellar anatomy and physiology. The model includes the main populations of the cerebellar cortex - Granular Cells (GrC), Golgi Cells (GoC), Molecular Layer Interneurons (MLI) and Purkinje Cells (PC) – and their connections. The connections among these neuronal populations include different excitatory, inhibitory or self-inhibitory synapses (Figure 1). Furthermore, we account for the multi-layer organization of the cerebellar cortex, where GrC layer and PC layer are the input and output layers, respectively[5]. The reference in functional terms is the spiking activity of neurons modelled as E-GLIF single-point neurons[6,7] optimized for each population . Population-specific firing frequencies and synaptic connections are used to calculate the conductance for each cell population (equations in Figure 1). A Transfer Function (TF) mathematical formalism[2] is used to transform population-specific spiking

patterns into a time-continuous global output. This approach is inspired to that already validated for the implementation of mean-field models of isocortical circuits made of excitatory and inhibitory neurons [9–11]. Here, the mean-field TF formalism accounts also for the physiological diversification of cerebellar neuronal populations and for their topological organization. GrCs and GoCs receive, through mossy fibers (mf), external synaptic input (ν_{input}) coming from other brain areas[5]. The detailed placement and connectivity generated by scaffold model approaches[8,12] are used to set connection probability (K). Detailed synaptic models (tuned and validated for each pairwise connection types) are used to set quantal synaptic conductances and synaptic time decays (Q, τ). Six different stationary ν_{input} (10, 20, 40, 60, 80, 100 Hz) are used to generate reference spiking activity in NEST for fitting the TFs.

PRELIMINARY RESULTS AND DISCUSSION

Figure1 shows the model structure and the conductance equation for each population with the explicit dependencies from the synaptic parameters K, Q and τ (values in Figure1-right). Figure2 shows our pipeline for PC. The color-map shows the behavior of the parameters used for TF fitting for either excitatory (ν_{GrC}) and inhibitory input activity (ν_{MLI}) to PC. The pipeline is extended to other populations. The final cerebellar mean-field formalism is reported in Figure2-right.

Compared to the existing mean field model, our cerebellar network is built up with a bottom-up approach tailored to the specific structural and functional interactions of the neurons population in the cerebellum.

This work aims, for the first time, to implement a mean-field model of cerebellum able to reproduce its population dynamics and to investigate specific cerebellar alterations in pathologies like ataxia and autism.
This design will allow to investigate, for each population, how its activity affects the cerebellar cortex output enabling a theoretical interpretation of network functions.

The spatial localization of input stimuli from the extended brain connectome will be fundamental to understand the topological organization of cerebellar signal processing. This will require multiple modules of this cerebellar mean field, each one receiving *mf*s from specific source regions. The differentiated descriptions of synapses connecting neuronal populations will allow to account for critical factors controlling local circuit dynamics (e.g. differentiation between AMPA and NMDA receptor at excitatory synapses, or between parallel fibers and ascending axons at GrC-GoC and GrC-PC synapses). Finally, to extend the model toward the mesoscale, the TF will be extended from the cerebellar cortex to include Deep Cerebellar Nuclei (DCN).
Once an interconnected set of cerebellar mean fields will be built and validated, it will be mapped on brain atlases and integrated in TVB, in order to exploit the long-range connectome. A recent work[13] demonstrated the importance of cerebellum in whole brain dynamics by focusing on cerebro-cerebellar loop Those results will be compared with those generated with the present ad-hoc mean field. TVB-NEST co-simulations are being developed to reproduce brain activity at different levels of granularity (e.g. with single neurons or populations resolution). It will be interesting to compare the change of brain dynamics when the cerebellum is modelled as a NEST spiking node in the full TVB or as the mean field node described here.

REFERENCES

[1] Pinotsis D, Robinson P, Graben PB, Friston K. Neural masses and fields: Modeling the dynamics of brain activity. Front. Comput. Neurosci. 2014;8(NOV):2013–2015.

[2] Boustani S El, Destexhe A. A master equation formalism for macroscopic modeling of asynchronous irregular activity states. Neural Comput. 2009;21(1):46–100.

[3] DiVolo M, Romagnoni A, Capone C, Destexhe A. Biologically Realistic Mena-Field Models of Conductance-Based Networks of Spiking Neurons with Adaptation. Neural 2019;31:653–680.

[4] D'Angelo E. Physiology of the cerebellum [Internet]. 1st ed. Elsevier B.V.; 2018.Available from: http://dx.doi.org/10.1016/B978-0-444-63956-1.00006-0

[5] Gandolfi D, Pozzi P, Tognolina M, et al. The spatiotemporal organization of cerebellar network activity resolved by two-photon imaging of multiple single neurons. Front. Behav. Neurosci. 2014;8(APR):1–16.

[6] Geminiani A, Casellato C, Locatelli F, et al. Complex dynamics in simplified neuronal models: Reproducing golgi cell electroresponsiveness. Front. Neuroinform. 2018;12(December):1–19.

[7] Geminiani A, Casellato C, D'Angelo E, Pedrocchi A. Complex electroresponsive dynamics in olivocerebellar neurons represented with extended-generalized leaky integrate and fire models. Front. Comput. Neurosci. 2019;13(June):1–12.

[8] De Schepper R, Al E. The Brain Scaffold Builder, a package for structural and functional modelling of brain circuits: the cerebellar use case. *In preparation*;

[9] Kuhn A, Aertsen A, Rotter S. Neuronal Integration of Synaptic Input in the Fluctuation-Driven Regime. J. Neurosci. 2004;24(10):2345–2356.

[10] Zerlaut Y, Chemla S, Chavane F, Destexhe A. Modeling mesoscopic cortical dynamics using a mean-field model of conductance-based networks of adaptive exponential integrate-and-fire neurons. J. Comput. Neurosci. 2018;44(1):45–61.

[11] Zerlaut Y, Destexhe A. Enhanced Responsiveness and Low-Level Awareness in Stochastic Network States [Internet]. Neuron 2017;94(5):1002–1009.Available from: http://dx.doi.org/10.1016/j.neuron.2017.04.001

[12] Casali S, Marenzi E, Medini C, et al. Reconstruction and simulation of a scaffold model of the cerebellar network. Front. Neuroinform. 2019;13(May):1–19.

[13] Palesi F, Lorenzi RM, Casellato C, et al. The Importance of Cerebellar Connectivity on Simulated Brain Dynamics. Front. Cell. Neurosci. 2020;14(July):1–11.

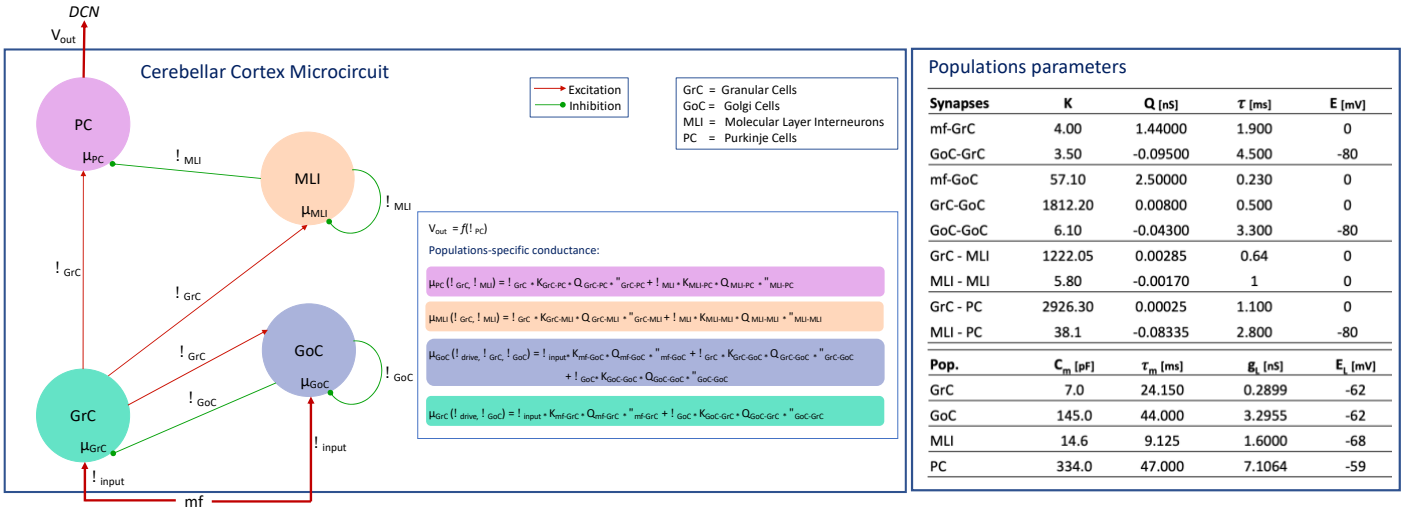

*Figure 1) Cerebellar cortex microcircuit model. The external input ν_{input} is relayed by mf to GrC and GoC. The output activity ν_{PC} projects to the DCN. ν_{input}=external input [Hz]; for each population p or connection c: m_p=conductance of each population [nS]; ν_p=firing rate of each population [Hz]; K_c=connections probability*cells numbers; Q_c = quantal synaptic conductance [nS], τ_c=synaptic time decay [ms]. p = GrC, GoC, MLI, PC. c = mf-GrC, mf-GoC, GrC-GoC, GoC-GrC, GoC-GoC, GrC-MLI, MLI-MLI, GrC-PC, MLI-PC.*

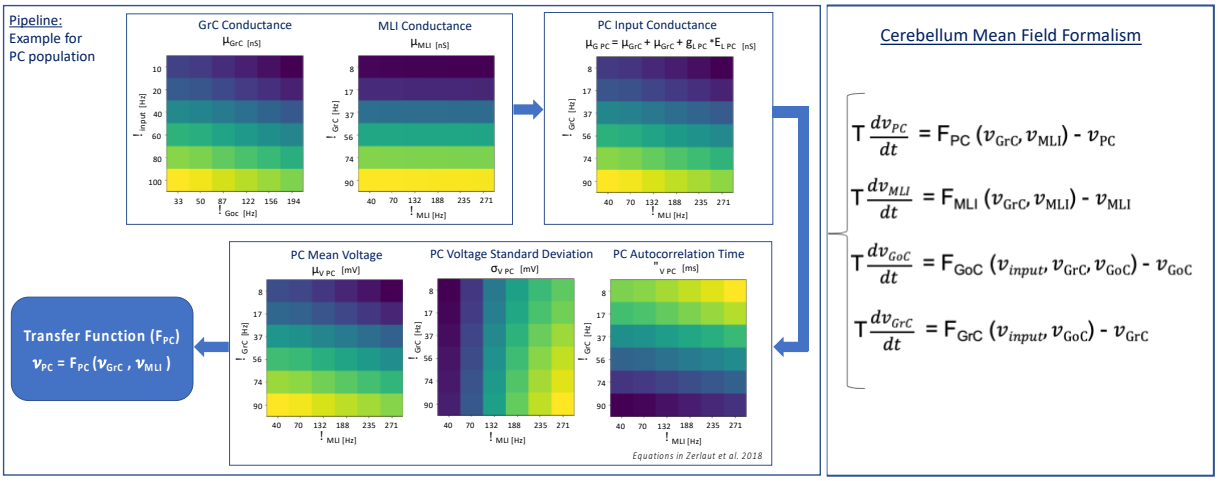

Figure 2) Pipeline to compute transfer function. Left: Color-map shows from yellow to blue the parameters used for Transfer Function Fitting. Population conductances assume high values for high excitations combined with low inhibition (Map bottom-left corner). PC m_V follows the same conductances trend, while σ_V is higher for low excitation and high inhibition. τ_V is higher for low excitation-high inhibition. Right: Cerebellum Mean Field Equations.

Effect of Psilocybin on neural oscillations and signal diversity in EEG and their psychological correlates

Faissal Sharif[1*], David Erritzoe[1], Laura Kärtner[1], Christopher Timmermann[1]

[1] Department of Brain Sciences, Faculty of Medicine, Imperial College London, London, United Kingdom
*fs419@ic.ac.uk

INTRODUCTION/MOTIVATION

Research interest in psychedelics has grown significantly in the last decade, with numerous studies exploring their ability to induce acute changes in states of consciousness [1]. These drastic physiological changes can translate into long-term psychological changes and could potentially be leveraged for psychotherapy [2,3,4]. As with all psychedelics, the effects of psilocybin, a tryptamine alkaloid contained in certain mushroom species, are mediated by serotonin 2A (5-HT2A) receptor agonism [5]. This mechanism has been implicated in the reduction of spectral power, particularly in the alpha band, as well as the increase of EEG signal diversity (entropy) under psychedelics [5,6,7]. Till date, few studies have replicated these findings and investigated their relationship with acute psychological effects of psilocybin. This study aimed to investigate the effects of high doses of psilocybin on spectral power, entropy, acute and long-term psychological effects such as emotional insight and ego dissolution, and how they are associated.

METHODS

In this within-subject study, 28 psychedelic-naive subjects received 1 mg (low dose, LD) and 25 mg (high dose, HD) of psilocybin, during two dosing days, four weeks apart. During each dosing day, four repeated acute measures of emotional insight, richness of imagery and strength of emotion were accompanied by resting-state EEG (RS-EEG) measures. Further, acute ego dissolution ratings and long-term changes in psychological insight at 2- and 4-weeks post-dosing were assessed. RS-EEG data was analysed for changes in power and entropy through Lempel-Ziv Complexity (LZs).

RESULTS AND DISCUSSION

All acute psychological measures were significantly increased in the HD compared to the LD. Similarly, long-term measures of psychological insight were increased after 25 mg psilocybin and stable over four weeks post-dosing. Widespread decreases in power were observed in alpha, and to a lesser extent, in theta and beta bands, after the HD and were accompanied by an increase of LZs (Figure 1, 2). Increases in gamma power correlated with acute measures of strength of emotion. Together, these findings largely support previous work on psychedelics and provide important insights into the neurobiological basis of the psychedelic experience under psilocybin, and their relation to acute and long-term psychological measures, further substantiating mechanistic aspects of psilocybin psychotherapy.

Keywords: Psychedelics, Psilocybin, EEG, Entropy, Lempel-Ziv, Alpha

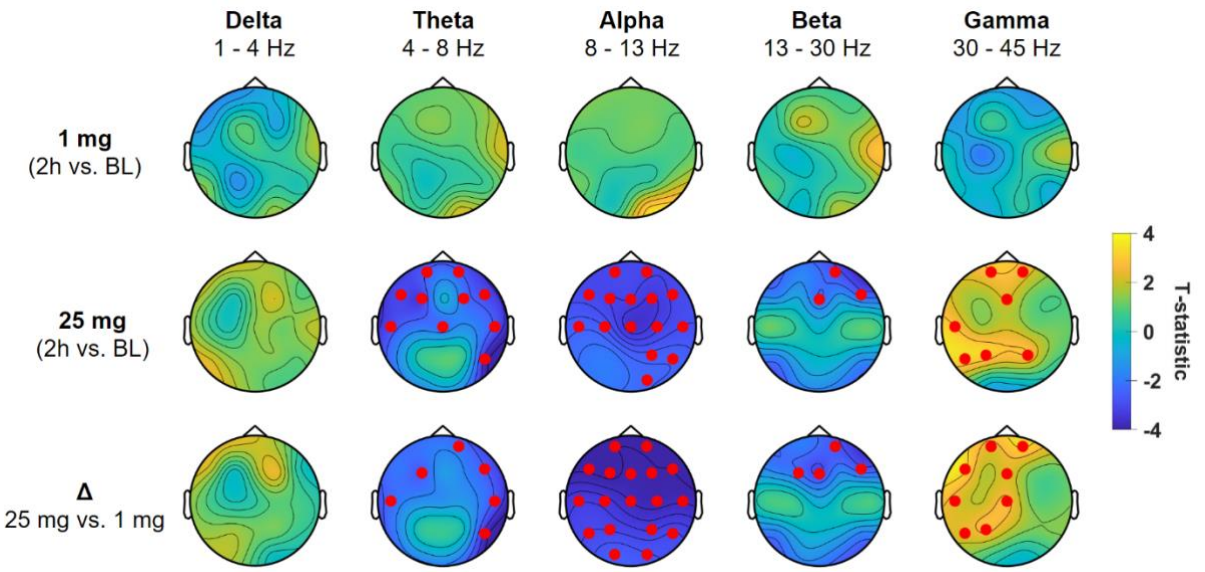

Figure 1. Topographic Spectral Power changes in LD and HD conditions (n = 19). Results of paired t-tests with false discovery rate (FDR) and cluster correction are presented. Comparisons of peak (2h post-dosing) vs. baseline spectral power in 1 mg, 25 mg, as well as comparisons between conditions (Δ) are shown. Significance is indicated as < .05 (red dot). Abbreviations: BL, baseline.

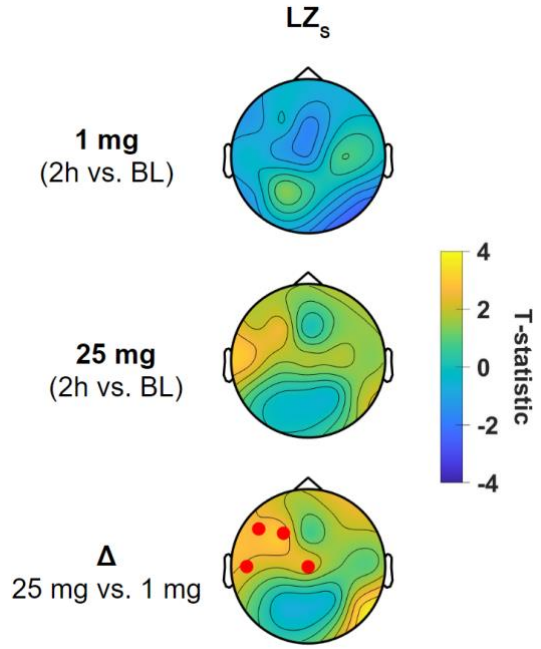

Figure 2. Topographic Lempel-Ziv Complexity changes in LD and HD conditions (n = 19). Results of t-tests with FDR and cluster correction are presented. Comparisons of peak (2h post-dosing) vs. baseline LZs activity in 1 mg, 25 mg, as well as comparisons between conditions (Δ) are shown. Significance is indicated as < .05 (red dot). Abbreviations: LZs , Lempel-Ziv Complexity; BL, baseline.

Acknowledgements: The author would like to thank Dr David Erritzøe and Laura Kärtner, who provided outstanding supervision and support throughout this project. Meg Spriggs, Dr Chris Timmermann and Dr Fernando Rosas provided crucial technical supervision and training on resting-state EEG data processing and analysis. University tuition and living expenses of the author have been funded entirely through the Klaus Murmann Fellowship Programme offered by the Foundation of German Business, under the umbrella of the Federal Ministry of Education and Research of Germany.

REFERENCES

[1] Heal, D.J., Henningfield, J., Frenguelli, B.G., Nutt, D.J., et al. (2018) Psychedelics - Re-opening the doors of perception. *Neuropharmacology*. 142, 1–6.

[2] Johnson, M.W., Garcia-Romeu, A., Cosimano, M.P. & Griffiths, R.R. (2014) Pilot study of the 5-HT2AR agonist psilocybin in the treatment of tobacco addiction. *Journal of psychopharmacology* . 28 (11), 983–992.

[3] Bogenschutz, M.P., Forcehimes, A.A., Pommy, J.A., Wilcox, C.E., et al. (2015) Psilocybin-assisted treatment for alcohol dependence: a proof-of-concept study. *Journal of psychopharmacology* . 29 (3), 289–299.

[4] Erritzoe, D., Roseman, L., Nour, M.M., MacLean, K., et al. (2018) Effects of psilocybin therapy on personality structure. *Acta psychiatrica Scandinavica*. 138 (5), 368–378.

[5] Carhart-Harris, R.L., Leech, R., Hellyer, P.J., Shanahan, M., et al. (2014) The entropic brain: a theory of conscious states informed by neuroimaging research with psychedelic drugs. *Frontiers in human neuroscience*. 8, 20.

[6] Muthukumaraswamy, S.D., Carhart-Harris, R.L., Moran, R.J., Brookes, M.J., et al. (2013) Broadband cortical desynchronization underlies the human psychedelic state. *The Journal of neuroscience: the official journal of the Society for Neuroscience*. 33 (38), 15171–15183.

[7] Timmermann, C., Roseman, L., Schartner, M., Milliere, R., et al. (2019) Neural correlates of the DMT experience assessed with multivariate EEG. *Scientific reports*. 9 (1), 16324.

II Brain organization, structure and function

Does the brain cause behaviour?

Abalo-Rodríguez, Inés[1], Estal-Muñoz, Víctor[2] and Pérez-Álvarez, Marino[3]

[1] Universidad Complutense de Madrid, Ctra. de Húmera, s/n, 28223 Pozuelo de Alarcón, Madrid (Spain)
[2] Universidad Autónoma de Madrid, Calle Iván Pavlov, 6, 28049 Madrid (Spain)
[3] Universidad de Oviedo, Calle San Francisco, 3, 33003 Oviedo, Asturias (Spain)
iabalo@ucm.es, victor.estal@uam.es, marino@uniovi.es

INTRODUCTION/MOTIVATION

Neuroscientists care about behaviour. According to the guidelines of the BRAIN project, "it is no exaggeration to say that nothing in neuroscience makes sense except in the light of behaviour" (p. 15) [1]. Therefore, it becomes essential to discuss the type of relationship that exists among the brain and behaviour. In multiple cases, this relationship is proposed to be causal, thus understanding the brain as the *cause* of behaviour. For instance, the objective III.4 of the BRAIN project, according to their guidelines, is in fact "demonstrating causality" of the brain over behaviour (p. 83). Other examples of this issue are the studies that attribute causality to the brain when talking about racist behaviour [2] or gender differences [3, 4]. Hence, the aim of this abstract is to critically analyse the correctness of attributing a causal role to the brain when talking about behaviour and under which circumstances, if any, it is in fact acceptable to do it.

METHODS

In this abstract, we are presenting a conceptual discussion of the causal role attributed to the brain over behaviour. Thus, the methodology employed will be the one used in philosophy. To this end, (1) we will first define *behaviour* in a broader sense, including both "internal cognitive processes" as well as externally observable actions. This conceptualization is in line with the suggestion made by several neuroscientists [e.g. 1] as well as the theoretical framework Behaviour Analysis [5, 6]. We will then (2) conceptualize what a *cause* is and what the requirements that need to be met in an experiment to conclude that "*A* causes *B"* are. These requirements are: (i) manipulation of A, (ii) randomization and (iii) temporal precedence of *A* over *B* [7, 8]. Finally, we will (3) revise the research conducted in neuroscience in the light of these requirements. In line with other authors [9], we will argue that the existing methodology does not meet the requirements (i) and (ii), and faces several difficulties when meeting (iii). Causal statements imply that we can directly control the variables of interests and randomize their conditions, which is unfortunately not the case when studying the brain. Moreover, the temporal precedence of the brain activity over the studied behaviour cannot be always ensured. This fact, together with the plasticity of the brain, raises the question of what the cause and the consequence are when studying the relationship among the brain and behaviour. Finally, (3) we will conclude that the existing methods and data allows us to talk about correlations but not causation.

RESULTS AND DISCUSSION

As a conclusion of the former points, we will argue that, while it is correct to understand the brain as the cause of behaviour under certain circumstances (e.g. in neurological disorders: a

brain malfunction *causes* an observed behavioural symptom such as loss of memory), we should be cautious when making these attributions in all the other cases. First of all, because of the aforementioned methodological limitations, which prevent us from making these interpretations. Correlation is not causation, and unfortunately enough, existing research on the brain does not generally enable us to establish a causal relationship over behaviour. Moreover, and more importantly, there is a theoretical mistake that should be avoided when interpreting these results. We should be aware that the brain activity that correlates with the observed behaviour is in fact a *description* at a biological level of that very same behaviour, rather than the *explanation*. Such a brain activity is of course necessary for that behaviour to happen, but attributing a causal role to it is in fact misleading [10, 11]. According to the well stablished framework of Behaviour Analysis, the cause of behaviour relies instead on the learning processes and history of the organism [5, 12]. Except from specific circumstances, the brain does *not cause*, but rather *enables* behaviour. Establishing such a distinction is essential in order to guide research in neuroscience and to properly interpret the phenomena that we are studying.

Keywords: brain, behaviour, cause, causal relationship, behaviour analysis

REFERENCES

[1] Bargmann, C., Newsome, W., Anderson, A., Brown, E., Deisseroth, K., Donoghue, J., & Sanes, J. (2014). BRAIN 2025: a scientific vision. Brain Research through Advancing Innovative Neurotechnologies (BRAIN) Working Group Report to the Advisory Committee to the Director, NIH.

[2] Smith, J. A., Marsh, J., & Mendoza-Denton, R. (2010). Are we born racist?: New insights from neuroscience and positive psychology. Beacon Press.

[3] Baron-Cohen, S. (2005, January). The essential difference: The male and female brain. In Phi Kappa Phi Forum (Vol. 85, No. 1, pp. 23-26). National Forum: Phi Kappa Phi Journal.

[4] Brizendine, L. (2006). The female brain. Broadway Books.

[5] Foxan-Parga, M. X. (Ed.) (2020). Análisis funcional de la conducta humana. Concepto, metodología y aplicaciones. Pirámide.

[6] Skinner, B. F. (1953). Science and human behavior. Simon and Schuster.

[7] Mosteller, F., & Tukey, J. W. (1977). Data analysis and regression: a second course in statistics.

[8] León, O. G., & Montero, I. (2003). Métodos de investigación en psicología y educación.

[9] Jazayeri, M., & Afraz, A. (2017). Navigating the Neural Space in Search of the Neural Code. Neuron, 93(5), 1003-1014.

[10] Fuchs, T. (2011). The brain--A mediating organ. Journal of Consciousness studies, 18(7-8), 196-221.

[11] Fuchs, T. (2017). Ecology of the brain: The phenomenology and biology of the embodied mind. Oxford University Press.

[12] Pérez Álvarez, M. (2011). El mito del cerebro creador: cuerpo, conducta y cultura.

Synaptology of human temporal neocortex: 3D-ultrastructural analyses

Nicolás Cano-Astorga[1,2], Javier DeFelipe[1,2,3], Lidia Alonso-Nanclares[1,2,3]

[1] Laboratorio Cajal de Circuitos Corticales, Universidad Politécnica de Madrid, Madrid, Spain.
[2] Instituto Cajal (CSIC) Madrid, Spain.
[3] Centro de Investigación Biomédica en Red sobre Enfermedades Neurodegenerativas (CIBERNED), Madrid, Spain.
*canoastorga.n@gmail.com

Introduction

Brain organization is extremely complex and our current knowledge it is far from being completed. The cerebral cortex attracts the researcher´s attention because is where cognitive process takes place. To understand how neuronal circuits contribute to the functional organization of the cerebral cortex, a detailed ultrastructural analysis of neuronal connectivity is required. In particular, Brodmann area 21 is involved in high-level cognitive functions like language [1]. This region is a highly connected cortex that integrates and distributes the information in many circuits [2]. These circuits are mainly established by cortico-cortical layer III projecting neurons, which process the information through synapses [3]. We have performed a detailed three-dimensional ultrastructural analysis of the neuropil, the region where most of the synapses are located. The goals of this study were to provide data about synaptic characteristics.

Methods

Human brain tissue samples were obtained from 8 control individuals (3 women and 5 men, whose ages ranged between 24 to 53 years old). Ultrastructural images were obtained using FIB/SEM, which removes 20 nm-thick layers of material and images the exposed surface. This procedure is continuously repeated, leading to fully reconstruct of a given volume [4]. The volume obtained by the FIB/SEM was analyzed using EspINA software [5]. Each synapse was individually identified and classified -by the user- as asymmetric (AS; excitatory) or symmetric (SS; inhibitory) based on its prominent or thin post-synaptic density, respectively [6] (Figure 1). Once a synapse was visually identified, EspINA reconstructs it semi-automatically in 3D. Based on this 3D reconstructed synapse, morphologic categories (macular, perforated, horseshoe or fragmented) were done attending to its shape [7]. EspINA also provides the area of the synaptic apposition surface (SAS) [8] and the position of its centroids [9], which allows analyzing the synaptic size and its spatial 3D distribution, respectively. Moreover, the postsynaptic targets (dendritic spines or dendritic shafts) of the synapses were clearly determined [10] (Figure 2).

Results and discussion

Preliminary results based on 11158 μm^3 examined tissue sample and 4945 synapses showed a mean synaptic density of 0.60 synapses/μm^3, most synapses were AS (93.33%) versus SS (6.67%), which concur with human related literature [11].

Macular-shape synapses were the most frequent (83.30%) following by perforated (11.69%), horseshoe (3.86%) and fragmented (1.15%), being the macular shape-synapses smaller than perforated, horseshoe and fragmented synapses, which concur with current hypothesis.

Furthermore, the spatial distribution study showed that synaptic spatial distribution pattern corresponds to a random pattern, in which the synapses can occupy any location of the space, which could be an intrinsic characteristic of cortical circuit´s organization. Finally, the study of the postsynaptic elements revealed that most AS were established on dendritic spines heads (66.7%), whereas most SS were established on dendritic shafts (90.1%). In the human cerebral cortex, it has been reported that the percentage of AS established on dendritic spines range between 47%-85% [12-15]. However, this percentage is about 80% in non-human primates [16-18], and 90% in rats and mice [10,17,19].

[1] Crigler, L. et al. (2006) 'Human mesenchymal stem cell subpopulations express a variety of neuro-regulatory molecules and promote neuronal cell survival and neuritogenesis', Experimental Neurology, 198(1), pp. 54–64. doi: 10.1016/j.expneurol.2005.10.029.

[2] Gögel, S., Gubernator, M. and Minger, S. L. (2011) 'Progress and prospects: stem cells and neurological diseases', Gene Therapy, 18(1), pp. 1–6. doi: 10.1038/gt.2010.130.

Bibliography

[1] Xu Y, Lin Q, Han Z, He Y, Bi Y. 2016. Intrinsic functional network architecture of human semantic processing: Modules and hubs. NeuroImage 132:42–55. DOI: https://doi.org/10.1016/j.neuroimage.2016.03.004

[2] Felleman DJ, Xiao Y, and McClendon E. 1997. Modular Organization of Occipito-Temporal Pathways: Cortical Connections between Visual Area 4 and Visual Area 2 and Posterior Inferotemporal Ventral Area in Macaque Monkeys. J Neurosci 17:3185-3200. DOI: https://doi.org/10.1523/JNEUROSCI.17-09-03185.1997

[3] Thomson A and Lamy C. 2007. Functional maps of neocortical local circuitry. Front in Neurosci 1:19-42. DOI: https://doi.org/10.3389/neuro.01.1.1.002.2007

[4] Merchán-Pérez A, Rodríguez JR, Alonso-Nanclares L, Schertel A, DeFelipe J. 2009. Counting synapses using FIB/SEM microscopy: a true revolution for ultrastructural volume reconstruction. Front Neuroanat 3:18. DOI: https://doi.org/10.3389/neuro.05.018.2009

[5] Morales J, Alonso-Nanclares L, Rodríguez JR, DeFelipe J, Rodríguez A, Merchán-Pérez A. 2011. Espina: a tool for the automated segmentation and counting of synapses in large stacks of electron microscopy images. Front Neuroanat 18:18. DOI: https://doi.org/10.3389/fnana.2011.00018

[6] Colonnier M. 1968. Synaptic patterns on different cell types in the different laminae of the cat visual cortex. An electron microscope study. Brain Res 9:268–287. DOI: https://doi.org/10.1016/0006-8993(68)90234-5

[7] Santuy A, Rodríguez J, DeFelipe J, Merchán-Pérez A. 2018a. Study of the size and shape of synapses in the juvenile rat somatosensory cortex with 3D electron microscopy. Eneuro 5:e0377-17. DOI: https://doi.org/10.1523/ENEURO.0377-17.2017

[8] Morales J, Alonso-Nanclares L, Rodríguez JR, DeFelipe J, Rodríguez A, Merchán-Pérez A. 2011. Espina: a tool for the automated segmentation and counting of synapses in large stacks of electron microscopy images. Front Neuroanat 18:18. DOI: https://doi.org/10.3389/fnana.2011.00018

[9] Merchán-Pérez A, Rodríguez JR, González S, Robles V, DeFelipe J, Larrañaga P, Bielza C. 2014. Three-dimensional spatial distribution of synapses in the neocortex: a dual-beam electron microscopy study. Cereb Cortex 24:1579–1588. DOI: https://doi.org/10.1093/cercor/bht018

[10] Santuy A, Rodriguez JR, DeFelipe J, Merchán-Pérez A. 2018b. Volume electron microscopy of the distribution of synapses in the neuropil of the juvenile rat somatosensory cortex. Brain Struct Funct 223:77–90. DOI: https://doi.org/10.1007/s00429-017-1470-7

[11] DeFelipe J, Alonso-Nanclares L, Arellano JI. 2002. Microstructure of the neocortex: Comparative aspects. J Neurocytol 31:299-316. DOI: https://doi.org/10.1023/a:1024130211265

[12] Yakoubi R, Rollenhagen A, von Lehe M, Shao Y, Sätzler K, Lübke JHR. 2018. Quantitative Three-Dimensional Reconstructions of Excitatory Synaptic Boutons in Layer 5 of the Adult Human Temporal Lobe Neocortex: A Fine-Scale Electron Microscopic Analysis. Cereb Cortex 29:2797–2814. DOI: https://doi.org/10.1093/cercor/bhy146

[13] Yakoubi R, Rollenhagen A, von Lehe M, Miller D, Walkenfort B, Hasenberg M, Sätzler K, Lübke JHR. 2019. Ultrastructural heterogeneity of layer 4 excitatory synaptic boutons in the adult human temporal lobe neocortex. eLife 20 8:e48373. DOI: https://doi.org/10.7554/eLife.48373

[14] Domínguez-Álvaro M, Montero-Crespo M, Blazquez-Llorca L, DeFelipe J, Alonso-Nanclares L. 2019. 3D Electron Microscopy Study of Synaptic Organization of the Normal Human Transentorhinal Cortex and Its Possible Alterations in Alzheimer's Disease. eNeuro 6:1-17. DOI: https://doi.org/10.1523/ENEURO.0140-19.2019

[15] Domínguez-Álvaro M, Montero-Crespo M, Blazquez-Llorca L, DeFelipe J, Alonso-Nanclares L. 2020. 3D ultrastructural study of synapses in the human entorhinal cortex. Cereb cortex bhaa233. DOI: https://doi.org/10.1093/cercor/bhaa233

[16] Peters A, Sethares C, Luebke JI. 2008. Synapses are lost during aging in the primate prefrontal cortex. Neurosci 152:970-981. https://doi.org/10.1016/j.neuroscience.2007.07.014

[17] Hsu A, Luebke JI, Medalla M. 2017. Comparative ultrastructural features of excitatory synapses in the visual and frontal cortices of the adult mouse and monkey. J Comp Neurol 525:2175–2191. DOI: https://doi.org/10.1002/cne.24196

[18] Dumitriu D, Hao J, Hara Y, Kaufmann J, Janssen WGM, Lou W, Rapp PR, Morrison JH. 2010. Selective changes in thin spine density and morphology in monkey prefrontal cortex correlate with aging-related cognitive impairment. J Neurosci. 30:7507-7515. https://doi.org/10.1523/JNEUROSCI.6410-09.2010

[19] Calì C, Wawrzyniak M, Becker C, Maco B, Cantoni M, Jorstad A, Nigro B, Grillo F, De Paola V, Fua P, Knott GW. 2018. The effects of aging on neuropil structure in mouse somatosensory cortex—A 3D electron microscopy analysis of layer 1. PLoS ONE 13:e0198131. DOI: https://doi.org/10.1371/journal.pone.0198131

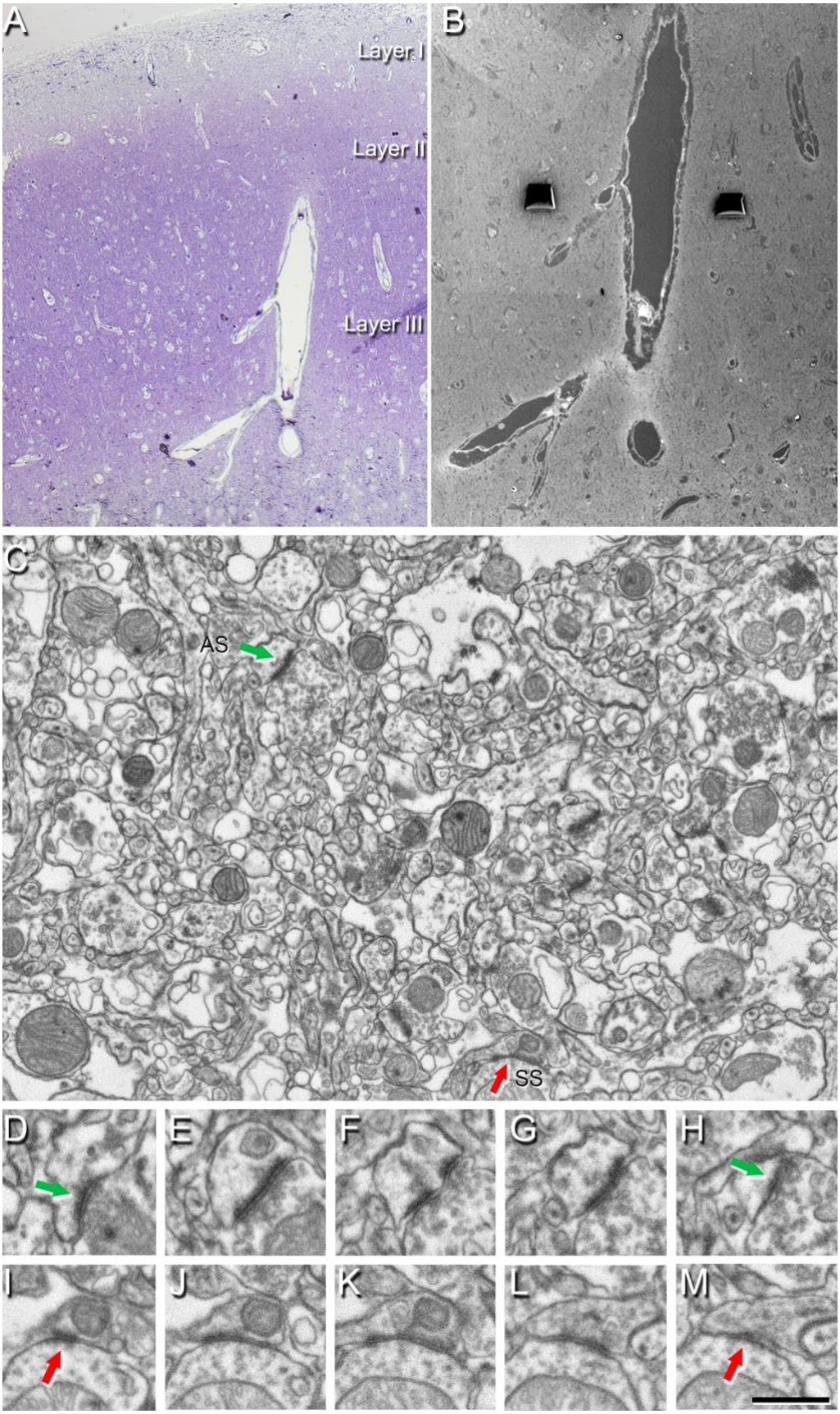

Figure 1.

Correlative light/electron microscopy analysis of layer III of the Brodmann area 21. (A) Delimitation of layers is based on the staining pattern of 1 µm-thick semithin section, stained with toluidine blue, which is adjacent to the block for FIB/SEM imaging (B). (B) SEM image with higher magnification of the blood vessels in A to illustrate the block surface with trenches made in the neuropil where FIB/SEM

analyses was performed. (C) Serial image obtained by FIB/SEM showing the neuropil of an autopsy case (AB3), two synapses are indicated as examples of asymmetric (AS, green arrow) and symmetric synapses (SS, red arrow). Synapse classification was based on the examination of the full sequence of serial images; an AS with prominent postsynaptic density can be visualized in D-H, and an SS with thin postsynaptic density, in I-M. Scale bar shown in M indicates 160 µm in A, 100 µm in B, 950 nm in C, and 550 nm in D-M.

Figure 2. FIB/SEM images from serial sections made in a biopsy case (H38) to illustrate a dendritic shaft

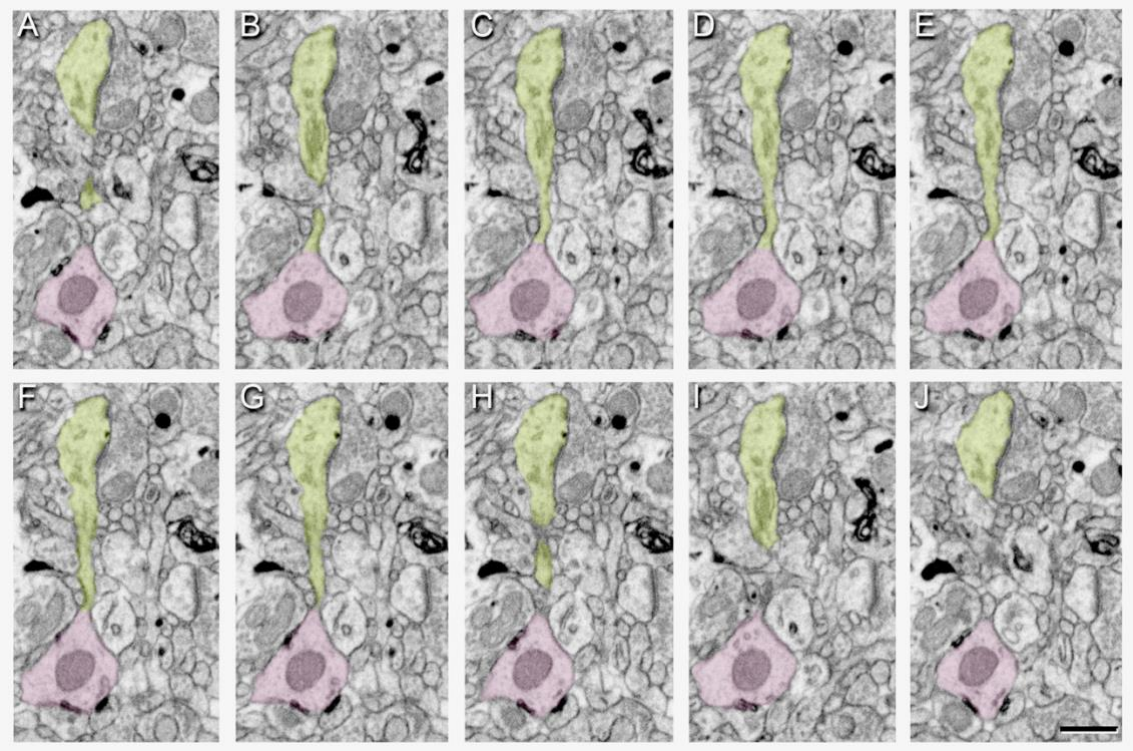

(pink) with one dendritic spine emerging from the shaft (in green). Scale bar shown in J indicates 500 nm in A-J.

Dephasing the speaking brain: Cleaning covert sentence production activation maps with a phase-based fMRI data analysis

Iñigo De Vicente[1], Eneko Uruñuela[1], Maite Termenon[1], César Caballero-Gaudes[1*]

[1] Basque Center on Cognition, Brain and Language, San Sebastián-Donostia, Spain
*c.caballero@bcbl.eu

INTRODUCTION/MOTIVATION

The spatial resolution in conventional gradient-echo functional MRI (fMRI) experiments is largely confounded by the blood-oxygenation level dependent (BOLD) signal changes emanating from large draining veins [1]. These macrovascular effects limit precise localization of the neuronal activity, which fundamentally occurs at the level of smaller veins and capillaries. Previous studies have observed that the phase of the fMRI signal captures BOLD changes in voxels with large vessels but not in voxels located within the microvasculature [2]. Thus, by performing a linear regression between the phase and magnitude BOLD signals, the signal contribution coming from large veins can be estimated, and subsequently removed from the original magnitude time-series. Here, we aim at investigating the performance of this phase-based denoising method on a covert sentence production task, where part of the observed activations in Broca's area may be biased towards macrovasculature contained in the Sylvian fissure [3]. We analyze the performance of two fitting algorithms, ordinary least-squares (OLS) [2] and orthogonal distance regression (ODR) [4], by comparing the conventional magnitude-based activation maps against those obtained after suppressing the contributions from macrovascular veins.

METHODS

T2*-weighted multiband gradient-echo echo-planar images (TR = 850ms, TE = 35ms, flip angle = 56º, multiband acceleration factor = 6, voxel size = 2.4 x 2.4 x 2.4 mm^3, matrix size = 88 x 88 mm^2, 452 volumes) were collected in 23 subjects in a fMRI experiment while they performed a covert sentence production task in Spanish [5]. All analyses were performed using AFNI [6] and in-house python scripts. Magnitude and phase fMRI signals were independently preprocessed prior to phase-based OLS [2] or ODR [4] denoising (which also required automatic filtering of respiratory-related fluctuations). Subject-level analyses were based on a general linear regression model which included the timings of the sentence production paradigm to model the task-evoked BOLD fluctuations, as well as the polynomials and motion-derived regressors to account for low-frequency trends and motion, and computed at the individual subject's space with 3dREMLfit to account for voxelwise temporal correlations. Separate GLM analyses were performed on the RAW preprocessed magnitude (i.e. without any phase-based denoising), and after the two phase-denoised methods (OLS-denoised and ODR-denoised). Group-level statistics comparing the different preprocessing strategies (RAW, OLS, ODR) were obtained with a mixed effects model using 3dMEMA [7].

RESULTS AND DISCUSSION

Both OLS and ODR algorithms estimated phase-magnitude correlations in similar regions, showing low coefficient of determination (R^2) values in white-matter voxels with reduced vasculature, and large R^2 values close to large veins, such as the superior sagittal sinus (see Figure 1). The R^2 maps matched the temporal standard deviation maps of the magnitude signal, which generally reflect physiological noise of large vessels. ODR outperformed OLS in terms of estimation accuracy, thus resulting in more effective removal of large draining effects. When comparing standard activation maps against those obtained after performing phase-based denoising, we found significant signal suppression in individual subjects and at the group-level (see Figure 2). As hypothesized, the larger effects of macrovascular contributions were observed in areas of the inferior frontal gyrus, particularly in the left pars orbitalis which is located adjacent to the Sylvian fissure and may thus contain large macrovascular signals. Our results demonstrate that previous covert sentence production studies can be biased towards macrovascular sources contained in the pars orbitalis. As such, we show that phase-based denoising methods have the potential to improve the accuracy of standard fMRI activation maps.

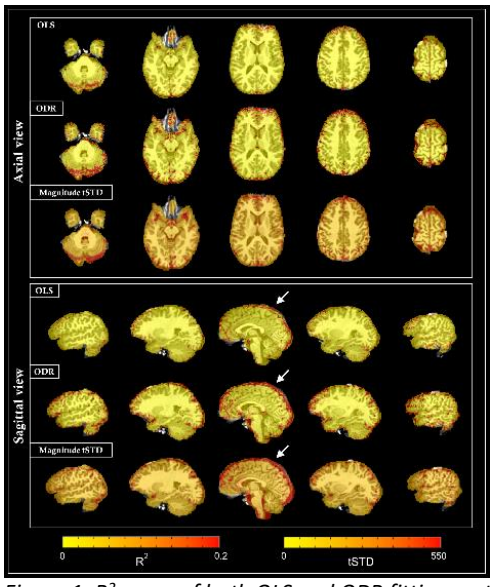

Figure 1: R^2 maps of both OLS and ODR fitting methods and temporal standard deviation (tSTD) map shown in the axial and sagittal planes for a representative subject. Arrows highlight the apparent pattern of the superior sagittal sinus.

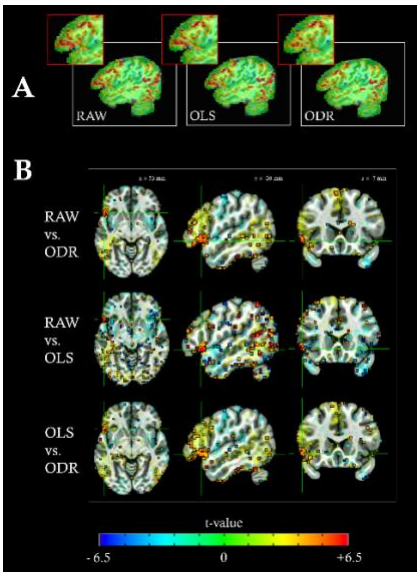

Figure 2: A) Sagittal slice showing activations from a representative subject at the left pars orbitalis. The activation maps correspond to: (left) RAW analysis, (middle) OLS phase-based denoising, (right) ODR phase-based denoising. B) Group-level effects of denoising in the activation maps at the left pars orbitalis. The maps depict significant differences using a mixed effects model between the analysis approaches: (top) RAW vs. ODR phase-based denoising, (middle) RAW vs. OLS phase-based denoising, (bottom) OLS vs. ODR phase-based denoising.

Keywords: Vein suppression, large draining veins, macrovascular bias, phase BOLD fMRI, phase regression, phase denoising, speech production

REFERENCES

[1] Hoogenraad, F. G., Hofman, M. B., Pouwels, P. J., Reichenbach, J. R., Rombouts, S. A., & Haacke, E. M. (1999). Sub-millimeter fmri at 1.5 tesla: correlation of high resolution with low resolution measurements. *Journal of Magnetic Resonance Imaging: An Official Journal of the International Society for Magnetic Resonance in Medicine*, 9(3), 475–482.

[2] Delion, M., Mercier, P., & Brassier, G. (2016). Arteries and veins of the sylvian fissure and insula: microsurgical anatomy. In *Advances and technical standards in neurosurgery* (pp. 185–216). Springer .

[3] Menon, R. S. (2002). Postacquisition suppression of large-vessel bold signals in high-resolution fmri. *Magnetic Resonance in Medicine: An Official Journal of the International Society for Magnetic Resonance in Medicine*, 47(1), 1–9.

[4] Curtis, A. T., Hutchison, R. M., & Menon, R. S. (2014). Phase based venous suppression in resting-state bold ge-fmri. *Neuroimage*, 100, 51–59.

[5] Mazoyer, B., Zago, L., Jobard, G., Crivello, F., Joliot, M., Perchey, G., ... & Tzourio-Mazoyer, N. (2014). Gaussian mixture modeling of hemispheric lateralization for language in a large sample of healthy individuals balanced for handedness. *PloS one*, 9(6), e101165.

[6] Cox, R. W. (1996). AFNI: software for analysis and visualization of functional magnetic resonance neuroimages. Computers and Biomedical research, 29(3), 162-173.

[7] Chen, G., Saad, Z. S., Nath, A. R., Beauchamp, M. S., & Cox, R. W. (2012). FMRI group analysis combining effect estimates and their variances. Neuroimage, 60(1), 747-765.

Morphological alterations of pyramidal neurons from the contralesional hemisphere after ischemic stroke

Sergio Plaza-Alonso[1,2], Asta Kastanauskaite[1,2], Susana Valero-Freitag[3], Nikolaus Plesnila[3], Farida Hellal[3], Javier DeFelipe[1,2,4] and Paula Merino-Serrais[1,2]

[1] Laboratorio Cajal de Circuitos Corticales, Centro de Tecnología Biomédica, Universidad Politécnica de Madrid, Madrid 28223, Spain.
[2] Instituto Cajal, Consejo Superior de Investigaciones Científicas (CSIC), Madrid 28002, Spain.
[3] Experimental Stroke Research, Institute for Stroke and Dementia Research, Cluster for Systems Neurology, University of Munich Medical Center, Munich, Germany.
[4] Centro de Investigación Biomédica en Red sobre Enfermedades Neurodegenerativas (CIBERNED), ISCII, Madrid, Spain.

INTRODUCTION

Stroke is one of the major causes of death and disability worldwide[1]. With over 80 million prevalent cases globally, the world is facing a modern epidemic[2].

Much emphasis has been placed on clarifying the pathological aspects and consequences of the focal lesion, the infarct core. However, interesting studies indicate that, after stroke, remote regions connected to the infarcted area are also affected. This process, known as diaschisis, is present among others, in the contralateral hemisphere, affecting the performance of the whole brain and may be implicated in the suppression of functional recovery after stroke[3–5].

Given this, the main goal of the present study was to analyze possible microanatomical alterations of pyramidal neurons in layer III from the contralesional somatosensory cortex-barrel field (BF) in the ischemic stroke mice model 'tMCAo'. These alterations could provide new insights into the understanding of the pathology and lead us to new therapy approaches.

METHODS

The transient middle cerebral artery occlusion mice stroke model (tMCAo) and the correspondent SHAM-control mice were used (20 weeks old, 18 male animals). 594 pyramidal neurons, located in the contralesional somatosensory cortex-barrel field (layer III) were individually injected with Lucifer Yellow (LY). LY injected cells were then 3D reconstructed using confocal microscopy and morphological parameters were analysed with Neurolucida 360 software[6] (Figure 1).

Several morphometric parameters were analysed in apical and basal dendritic trees. First, we evaluated the complexity of the dendritic arborization in both, apical and basal dendritic tree by measuring: dendritic length; dendritic volume; number of intersections; dendritic surface; number of nodes and dendritic diameter, as a function of the distance from the soma (Sholl analysis - 30 cells per group). This analysis creates a 3D scaffold of concentric spheres that normalize measures, thus allowing a reliable comparison between groups (Figure 1C).

Then, spine morphology was analysed through different morphometric parameters, such as dendritic spine density; dendritic spine length and dendritic spine volume, in apical and basal dendritic trees. This data was studied as a function of the distance from the soma (Sholl analysis), as an average per dendrite and as a frequency distribution analysis (minimum of 21 dendrites per group).

Statistical analysis: Mann-Whitney test was used to compare averages (mean ± SEM); Kolmogorov – Smirnov test was used in the frequency distribution analysis; Two-way ANOVA

followed by a post–hoc Bonferroni comparison was used to compare values when presented as a function of the distance from the soma (Sholl analysis).

Results/discussion

Apical dendritic tree shows less neuronal complexity in tMCAo animals: significant decrease in dendritic length (Figure 2A), number of intersections (Figure 2C), and dendritic surface (Figure 2D) of the apical dendritic tree were found in tMCAo compared with SHAM mice. No changes were found in basal dendritic tree analysis in any parameter.

Apical and basal dendrites show alterations in spine morphology: Frequency distribution analysis reveals significant changes in spine length and volume in both apical and basal dendritic trees between groups. No differences were found in Sholl and average analysis.

The complexity of the neuronal dendritic structure determines their biophysical properties, thus influencing their functional capacity and potential for plastic change. In addition, dendritic spines, being the main post-synaptic element, are targets of most excitatory synapses in the cerebral cortex and their morphology could determine synaptic strength and learning rules[7–9]. Therefore, alterations of spine morphology and neuronal complexity could affect neuronal function. Furthermore, the morphological alterations found in this study could play an important role in the recovery of the patient, since most of the post-ictus rehabilitation therapies rely on the neuronal and circuit potential for plasticity of the areas both close to the infarct core and symmetrically located in the contralateral hemisphere[10,11]. Thus, the alterations found in this stroke model are of great interest and should be further analysed. In fact, we are currently extending the areas of study to perform these analyses. Specifically, we are planning to include the contralateral hippocampus and the secondary somatosensory cortex, both areas in which the ischemic lesion may have a different impact.

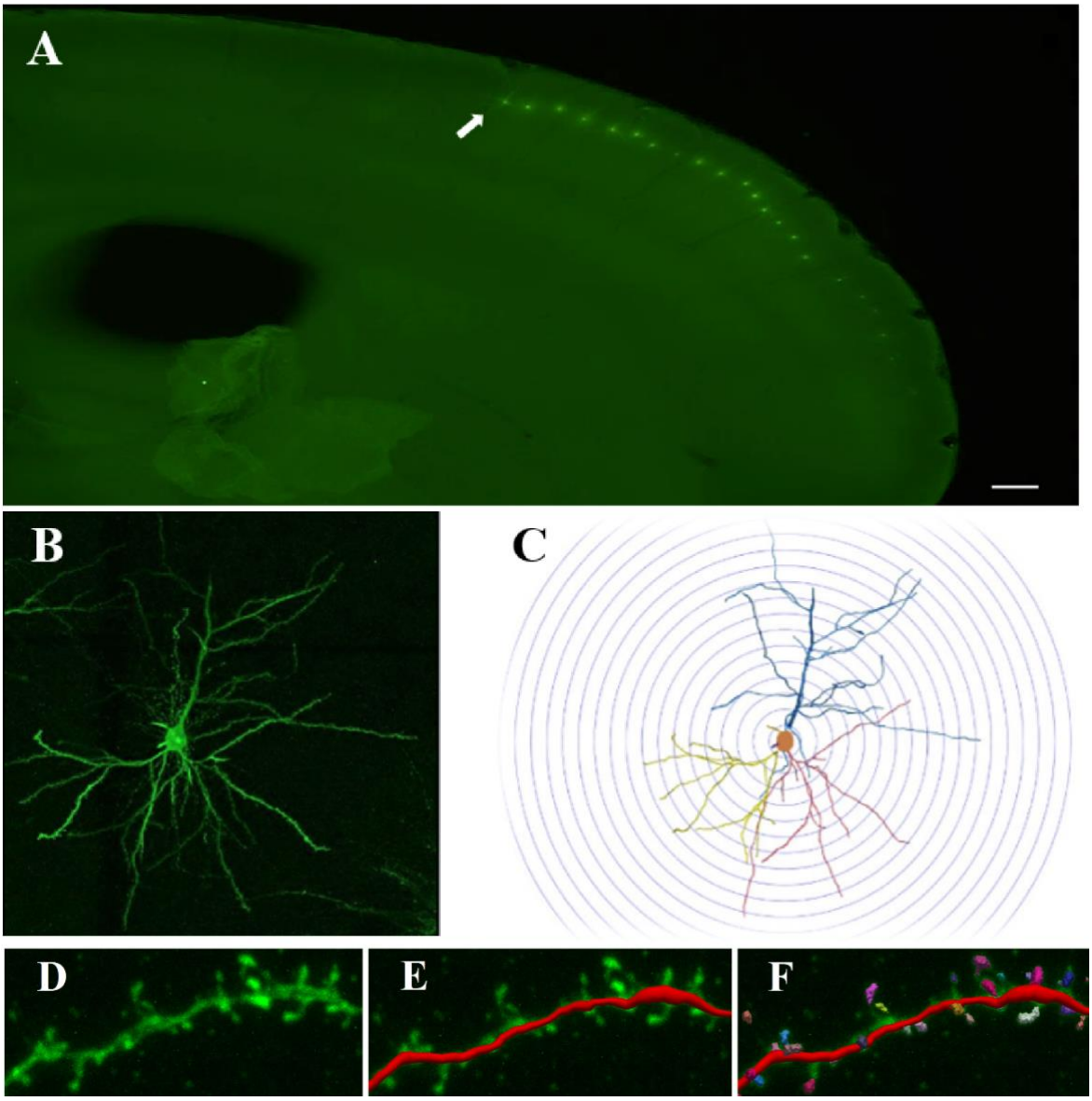

Figure 1. A) Panoramical overview of LY injected pyramidal neurons (in green) from a SHAM somatosensory cortex transversal section (right hemisphere). B). Detail of a LY injected neuron from Fig 1A. (indicated with a white arrow). Neuronal and spine structure were 3D reconstructed using confocal microscopy and visualizce with Neurolucida 360 software. C). 3D tracing model of the pyramidal neuron from Fig. 1B. Concentric spheres represent the segments made by Sholl Analysis to estimate the data. D) Detail of a LY injected apical dendrite from a SHAM mouse. E-F). 3D trace of the dendrite branch (in red) and dendritic spines from Fig 1D.

Apical Dendritic Tree Complexity: Sholl Analysis

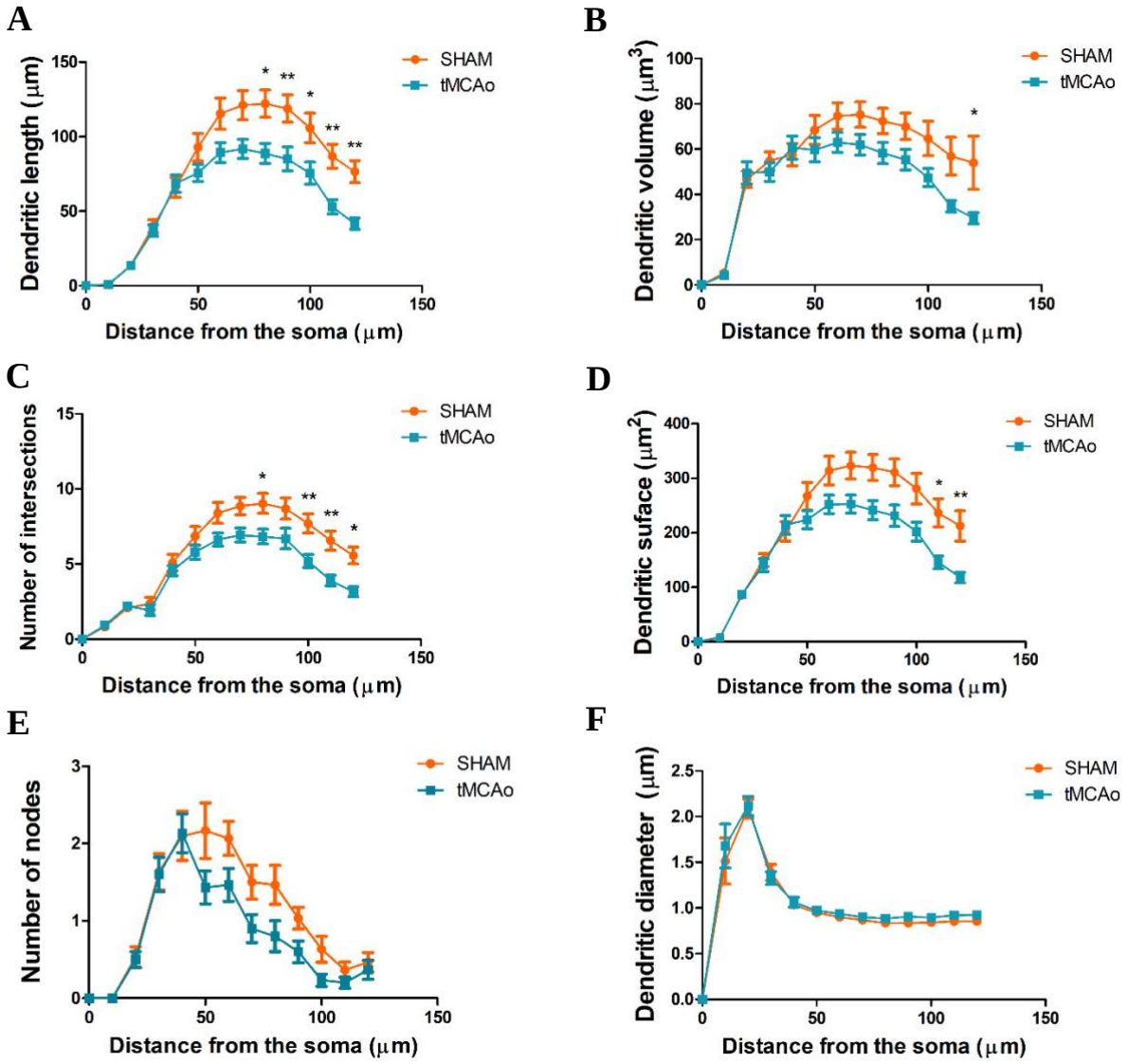

*Figure 2. Reduction in the apical dendritic tree complexity. Results from Apical Dendritic Tree morphological Sholl analysis. Significant decreases were found in several parameters (Dendritic Length; Number of intersection; Dendritic Surface and Dendritic Volume) from tMCAo mice model, compared to SHAM. Two-way ANOVA (repeated measures) and post-hoc Bonferroni test were used to analyze the data. N= 30 cells per group (tMCAo, SHAM). Data is shown as mean ± SEM. *p<0.05; **p<0.01*

REFERENCES

[1] Donnan GA, Fisher M, Macleod M, Davis SM. Stroke. Lancet (London, England). 2008 May;371(9624):1612–23.

[2] Global, regional, and national burden of neurological disorders, 1990-2016: a systematic analysis for the Global Burden of Disease Study 2016. Lancet Neurol. 2019 May;18(5):459–80.

[3] Buetefisch CM. Role of the Contralesional Hemisphere in Post-Stroke Recovery of Upper Extremity Motor Function. Front Neurol. 2015;6:214.

[4] Duering M, Righart R, Csanadi E, Jouvent E, Hervé D, Chabriat H, et al. Incident subcortical infarcts induce focal thinning in connected cortical regions. Neurology. 2012 Nov;79(20):2025–8.

[5] Silasi G, Murphy TH. Stroke and the connectome: how connectivity guides therapeutic intervention. Neuron. 2014 Sep;83(6):1354–68.

[6] Benavides-Piccione R, Regalado-Reyes M, Fernaud-Espinosa I, Kastanauskaite A, Tapia-González S, León-Espinosa G, et al. Differential Structure of Hippocampal CA1 Pyramidal Neurons in the Human and Mouse. Cereb Cortex. 2019 Jul 2.

[7] Benavides-Piccione R, Fernaud-Espinosa I, Robles V, Yuste R, DeFelipe J. Age-based comparison of human dendritic spine structure using complete three-dimensional reconstructions. Cereb Cortex. 2013 Aug;23(8):1798–810.

[8] van Elburg RAJ, van Ooyen A. Impact of Dendritic Size and Dendritic Topology on Burst Firing in Pyramidal Cells. PLOS Comput Biol. 2010 May 13;6(5):e1000781.

[9] Stuart GJ, Spruston N. Dendritic integration: 60 years of progress. Nat Neurosci. 2015 Dec;18(12):1713–21.

[10] Carmichael ST. Plasticity of cortical projections after stroke. Neuroscientist. 2003 Feb;9(1):64–75.

[11] Gerloff C, Bushara K, Sailer A, Wassermann EM, Chen R, Matsuoka T, et al. Multimodal imaging of brain reorganization in motor areas of the contralesional hemisphere of well recovered patients after capsular stroke. Brain. 2005 Dec 19;129(3):791–808.

Investigating non-invasive deep brain stimulation using temporally interfering electric fields

Dimitrios Stoupis[1*]

[1] Department of Physics, Aristotle University of Thessaloniki, Greece
[*]dstoupis@auth.gr

INTRODUCTION/MOTIVATION

Treating brain diseases or suppressing their symptoms by electric stimulation is not a trivial task. Different methods exist for stimulating structures deep in the brain, but usually these are invasive, posing considerable risk for the overall health of the individual. This is one of the main reasons there is wide research activity in non-invasive methods for deep brain stimulation. The problem of most non-invasive methods is the lack of focality to stimulate a small target area. An emerging technique in the field of applied neuroscience is the Transcranial Temporal Interference Stimulation (tTIS), showing promising results [1], [2]. The great advantage of this method is the high penetration depth it can achieve, without affecting the surrounding areas, thus making it ideal for targeted deep brain stimulation. The benefits of this method can be utilized to study the response pattern through EEG signals by stimulating a very small area of choice non-invasively. The current work presents the development of a software tool capable of importing realistic human head models derived from medical imaging data and creating a personalized treatment plan for tTIS. This work is ongoing with the aim of optimizing the treatment plan of the tTIS to stimulate specific targets inside the brain.

METHODS

The software tool was developed in Python and it is available in GitLab [3]. Initially, to verify the code that has been developed, a replication simulation was run on the sphere model reported in [1]. Subsequently, the code was applied in anatomically realistic models taken from the Population Head Model repository (PHM) [4], [5]. More specifically, all the models were meshed with the help of the PyMesh library using a tetrahedral mesh suitable for the implementation of the Finite Element Method (FEM). The electrodes were placed on the surface of the head, following the 10-20 international standard, using the code developed by [6]. Eventually, the Laplace equation was solved to extract the potential in the different areas of the model and the resulting internal electric field, by utilizing the FEM solvers of SfePy [7]. The dielectric properties of the tissues used in the models were taken from [8] at the frequency of 1 kHz used for creating the temporal interference in the PHM.

RESULTS AND DISCUSSION

There was very good agreement between the results obtained in [1] inside the sphere model and the results with the code developed in this work (**Figure 6**), therefore the code can be considered as validated/verified.

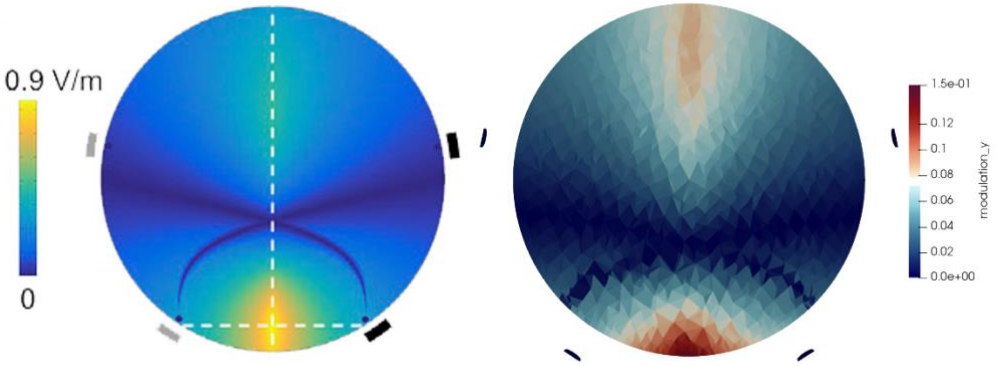

Figure 6: Comparison of the results from Grossman et al. (left) and the present work(right)
The result of the temporal interference envelop, using electrodes P4, F7 for the VCC and GND, respectively, of the first frequency pair (1 kHz) and electrodes P3, F8 for the second frequency pair (1.04 kHz) can be seen in Figure 7. One important observation that came up from the results obtained with PHM is that, as expected, the distribution of the electric field varies significantly between different models, using the same electrode pair (of the 10-20 system). Therefore, optimization methods need to be applied to maximize the electric field in deep areas of interest in the brain. This optimization will be performed in the near future for the different head models of the PHM [4], [5] to study the variations and the difficulties or traits that will arise.

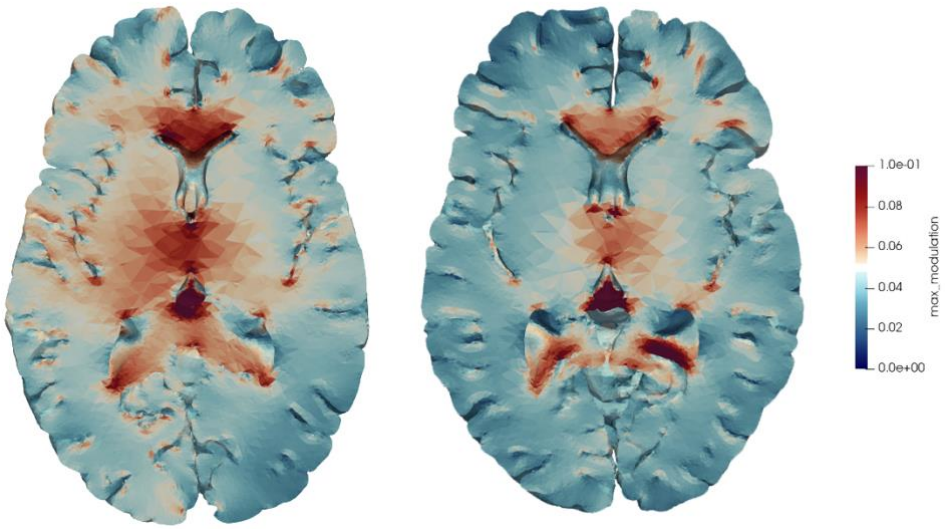

Figure 7: Comparison of the temporal interference envelop, using electrodes P4, F7 for the VCC and GND respectively of the first frequency pair (1 kHz) and electrodes P3, F8 for the second frequency pair (1.04 kHz), based on the 10-20 standard

Keywords: neuroscience, temporal interference, finite elements, deep brain stimulation

ACKNOWLEDGEMENTS: This research work is part of the author's thesis, supervised by Prof. Theodoros Samaras.

The results presented in this work have been produced using the Aristotle University of Thessaloniki (AUTh) High Performance Computing Infrastructure and Resources.

REFERENCES

[1] N. Grossman, D. Bono, N. Dedic, S. B. Kodandaramaiah, A. Rudenko, H.-J. Suk, A. M. Cassara, E. Neufeld, N. Kuster, L.-H. Tsai, A. Pascual-Leone and E. S. Boyden, "Noninvasive Deep Brain Stimulation via Temporally Interfering Electric Fields," Cell, vol. 169, p. 1029–1041.e16, 6 2017.

[2] S. Rampersad, B. Roig-Solvas, M. Yarossi, P. P. Kulkarni, E. Santarnecchi, A. D. Dorval and D. H. Brooks, “Prospects for transcranial temporal interference stimulation in humans: A computational study,” NeuroImage, vol. 202, p. 116124, 11 2019.

[3] D. Stoupis, “tACS Temporal Interference - Project ID: 18467592,” [Online]. Available: https://gitlab.com/dimst23/tacs-temporal-interference. [Accessed 5 11 2020].

[4] E. G. Lee, W. Duffy, R. L. Hadimani, M. Waris, W. Siddiqui, F. Islam, M. Rajamani, R. Nathan and D. C. Jiles, “Investigational Effect of Brain-Scalp Distance on the Efficacy of Transcranial Magnetic Stimulation Treatment in Depression,” IEEE Transactions on Magnetics, vol. 52, p. 1–4, 7 2016.

[5] E. G. Lee, P. Rastogi, R. L. Hadimani, D. C. Jiles and J. A. Camprodon, “Impact of non-brain anatomy and coil orientation on inter- and intra-subject variability in TMS at midline,” Clinical Neurophysiology, vol. 129, p. 1873–1883, 9 2018.

[6] P. Giacometti, K. L. Perdue and S. G. Diamond, “Algorithm to find high density EEG scalp coordinates and analysis of their correspondence to structural and functional regions of the brain,” Journal of Neuroscience Methods, vol. 229, p. 84–96, 5 2014.

[7] R. Cimrman, V. Lukeš and E. Rohan, “Multiscale finite element calculations in Python using SfePy,” Advances in Computational Mathematics, vol. 45, p. 1897–1921, 5 2019.

[8] C. Gabriel, “Compilation of the Dielectric Properties of Body Tissues at RF and Microwave Frequencies.,” Defense Technical Information Center, 1996.

A homeostatic mechanism for plasticity in heterogeneous spiking networks

Timo Gierlich[1*], Akos F. Kungl[1], Andreas Baumbach[1], Mihai A. Petrovici[12]

[1] Kirchhoff Institute for Physics, Heidelberg University, Heidelberg, Germany
[2] Department of Physiology, University of Bern, Bern, Switzerland
*gierlich@kip.uni-heidelberg.de

INTRODUCTION/MOTIVATION

Even compared to today's computer architectures, the human brain keeps impressing us with its robustness, speed, low-energy consumption and learning capabilities. Understanding these properties at a mechanistic level that is on the level of neurons and synapses and capturing these advantages in neuromorphic hardware [1, 2] is still an ongoing quest. A major challenge on the way is noise and parameter variability. To increase both biological plausibility and hardware compatibility, models need to take into account that neuronal systems show inherent parameter variation [3, 4, 5] and omnipresent temporal noise, which requires a large degree of computational robustness. Hence, robust learning rules are required to compensate for this variability and to enable reliable operation and learning. Further, homeostatic mechanisms are crucial to keep the neural network in its working regime and to compensate for variations in the environment [6]. In this work, we address this problem within a model of spike-based Bayesian inference. We propose an anti-Hebbian spike-timing-dependent plasticity (STDP) learning rule that could keep the effect of reciprocal synaptic connections between two neurons symmetric, which is often an implicit but important assumption in models of the brain [7, 8, 9].

METHODS

Recent work suggests that the human brain executes perception based on Bayesian inference on noisy and ambiguous input data [10, 11]. The neural sampling theory interprets the brain's neural activity as a sampling process from a probability distribution that represents a learned model of our environment [8, 10] (fig. 1b). In this theory, we view the neural activity as a process of scanning over network-states whereby the time spent in a certain state is proportional to its probability. Our approach uses a model of sampling with spiking neurons (fig 1a) [8, 9, 12, 13]. This model requires the effect of reciprocal synaptic connections to be symmetric, which a priori may not be the case both in biological neural networks and analog neuromorphic substrates. Moreover, in a local learning rule weight updates also need to be symmetric, which is not necessarily fulfilled in heterogeneous systems, because the plasticity mechanisms belonging to each synapse are physically distinct (fig. 1c and d). Consequently, a robust learning rule should incorporate a symmetrization mechanism to fulfill the requirement of the ideal abstract model.

In this work, we propose an anti-Hebbian learning algorithm based on STDP [14] that can establish homeostasis during training (fig. 2a, orange curve). We simulated the networks with SBS [15], a python framework for spike-based sampling using the numerical simulator NEST [16].

RESULTS AND DISCUSSION

We consider a two-neuron system with the connection from neuron 1 to neuron 2 W_{21} being larger than the reciprocal connection W_{12}. On average, neuron 2 will spike more often directly

after neuron 1 than vice versa (fig. 2a, blue curve), which results in a net negative update of W_{21} (and a positive one of W_{12}) and hence move the two weights closer to each other.
Numerical simulations of a two-neuron system consisting of stochastic spiking neurons connected by unequal weights revealed that the symmetrization algorithm only functions for equal bias or zero mean weight (see fig 2b and c). For example, in the regime of high positive weights, the algorithm results in a solution where the weight from the low-bias neuron to the high bias neuron is stronger than its reciprocal counterpart. This happens because the exponential shape of the postsynaptic potential makes the instantaneous firing rate of the postsynaptic neuron peak directly after the incoming spike. We conclude that the unequal base firing rates of the neurons together with this strong non-linear response gives rise to this unexpected behavior.
Our preliminary results suggest that an appropriate choice of STDP kernels (instead of the exponential in the original scheme) could mitigate this effect. Above that, classical tools from machine learning such as regularization and sparsity targets could help to keep the weights small while conserving activity in the hidden layer.
Until now, implementations of sampling on neuromorphic hardware [13, 17, 18] relied on the time-consuming computation of model parameter updates on an external CPU. To exploit the energy and speed advantages of neuromorphic hardware, we aim for a fully on-chip implementation of spike-based sampling together with a local STDP-based learning rule and a symmetrization mechanism on the BrainScaleS-2 neuromorphic platform [19].

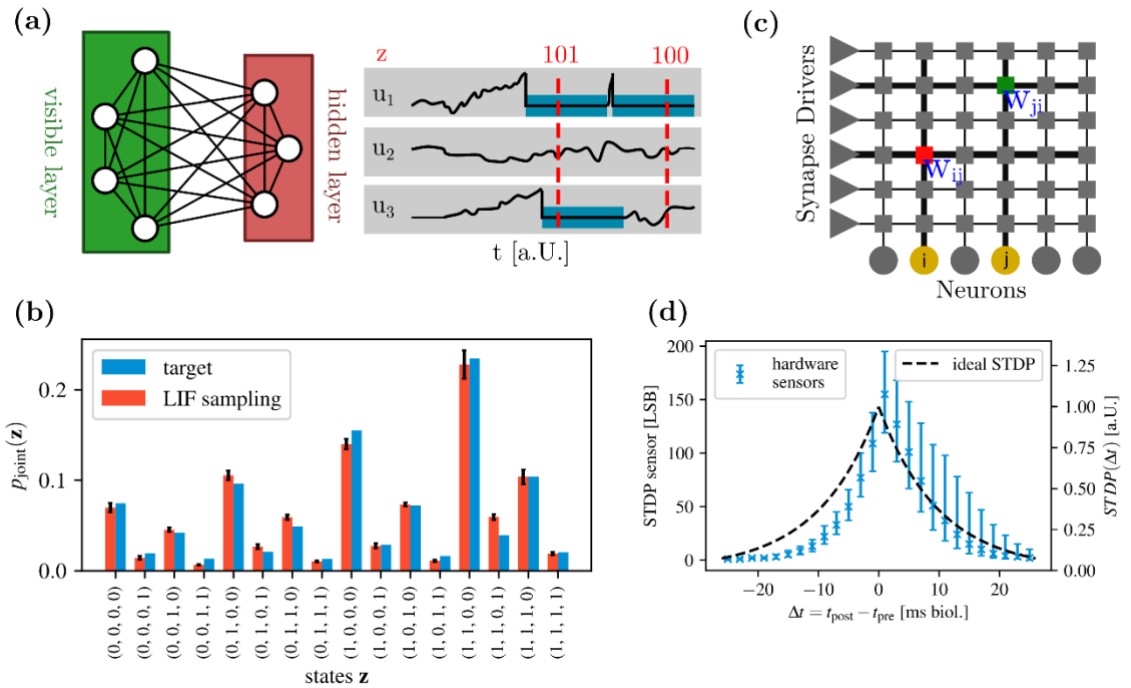

Figure 8 (a) Left: Exemplary architecture of a sampling network. Right: The dynamics of the membrane potentials of leaky integrate-and-fire neurons are interpreted as binary states. If a neuron is refractory (blue shaded part), it is identified with z=1, otherwise with z=0. (b) Illustration of sampling: A high-dimensional probability distribution (blue) is sampled via the dynamics of the spiking network. (c) Illustration of the implication of a heterogeneous substrate on the required symmetry of a network: In a neuromorphic hardware, for example, reciprocal connections are made of distinct synapse and neuron circuits. (d) Measurements of a symmetric STDP curve in the BrainScaleS-2 neuromorphic system [20] show considerable variations.

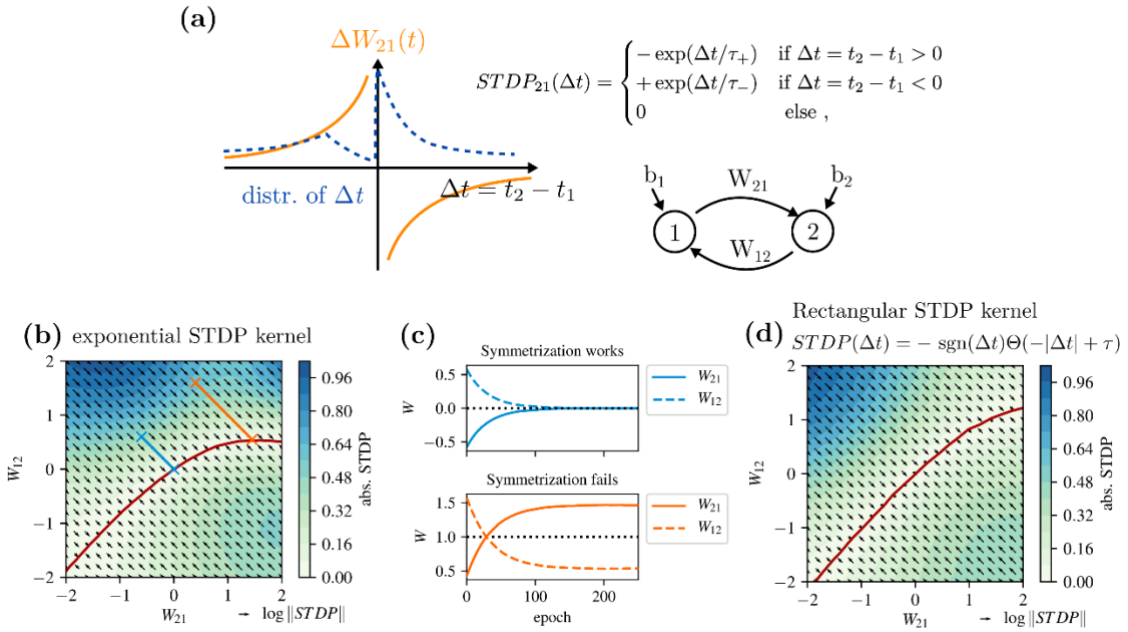

Figure 9 (a) Motivation of the symmetrization algorithm. Distribution of intervals between spikes from presynaptic neuron 1 to postsynaptic neuron 2 (blue dashed line). Here, $W_{21} > W_{12}$, which results in many small positive intervals and hence, many large negative updates. Weighting the blue curve with the anti-symmetric exponential kernel (orange) results in a net negative weight update for W_{21}. (b) Phase plane diagram of weight updates with exponential STDP kernel. For a fixed set of biases $b_1 = 1.0$ and $b_2 = 0.0$ we calculate the weight update for every combination of W_{12} and W_{21}. The arrows indicate the direction of the update, while the colormap in the background marks its absolute value. The stable attractor plotted in the red — this is where the algorithm converges to — deviates from the diagonal, which would be the desired outcome. (c) Time evolution of symmetrization. The trajectories are marked in (c). (d) Phase plane diagram with a rectangular STDP kernel. An appropriate kernel choice can mitigate the deviation from the desired symmetric outcome.

Keywords: learning, plasticity, spiking neurons, heterogeneous systems, homeostasis, Bayesian inference, sampling, neuromorphic hardware

Acknowledgements: This work has received funding from the European Union 7 th Framework Programme under grant agreement 604102 (HBP), the Horizon 2020 Framework Programme under grant agreements 720270, 785907, 945539 (HBP) and the Manfred Stärk Foundation, Germany. The authors acknowledge support by the state of Baden-Württemberg through bwHPC and the German Research Foundation (DFG) through grant no INST 39/963-1 FUGG (bwForCluster NEMO).

REFERENCES

[1] Roy, Kaushik, Akhilesh Jaiswal, and Priyadarshini Panda. 2019. “Towards Spike-Based Machine Intelligence with Neuromorphic Computing.” Nature 575 (7784): 607–17. https://doi.org/10.1038/s41586-019-1677-2.

[2] Schuman, Catherine D., Thomas E. Potok, Robert M. Patton, J. Douglas Birdwell, Mark E. Dean, Garrett S. Rose, and James S. Plank. 2017. “A Survey of Neuromorphic Computing and Neural Networks in Hardware,” May. http://arxiv.org/abs/1705.06963.

[3] Marder, Eve, and Jean Marc Goaillard. 2006. “Variability, Compensation and Homeostas in Neuron and Network Function.” Nature Reviews Neuroscience 7 (7): 563–74. https://doi.org/10.1038/nrn1949.

[4] Pfeil, Thomas, Andreas Grübl, Sebastian Jeltsch, Eric Müller, Paul Müller, Mihai A. Petrovici, Michael Schmuker, Daniel Brüderle, Johannes Schemmel, and Karlheinz Meier 2013. “Six Networks on a Universal Neuromorphic Computing Substrate.” Frontiers in Neuroscience 7 (7 FEB): 1–17. https://doi.org/10.3389/fnins.2013.00011.

[5] Petrovici, Mihai A., Bernhard Vogginger, Paul Müller, Oliver Breitwieser, Mikael Lundqvi Lyle Muller, Matthias Ehrlich, et al. 2014. “Characterization and Compensation of Netwc Level Anomalies in Mixed-Signal Neuromorphic Modeling Platforms.” PLoS ONE 9 (10). https://doi.org/10.1371/journal.pone.0108590.

[6] Zenke, Friedemann, Guillaume Hennequin, and Wulfram Gerstner. 2013. “Synaptic Plasticity in Neural Networks Needs Homeostasis with a Fast Rate Detector.” PLoS Computational Biology 9 (11). https://doi.org/10.1371/journal.pcbi.1003330.

[7] Hopfield, John J. 2018. “Neural Networks and Physical Systems with Emergent Collective Computational Abilities.” Feynman and Computation 79 (April): 7–19. https://doi.org/10.1201/9780429500459.

[8] Buesing, Lars, Johannes Bill, Bernhard Nessler, and Wolfgang Maass. 2011. “Neural Dynamics as Sampling: A Model for Stochastic Computation in Recurrent Networks of Spiking Neurons.” PLoS Computational Biology 7 (11). https://doi.org/10.1371/journal.pcbi.1002211.

[9] Petrovici, Mihai A., Johannes Bill, Ilja Bytschok, Johannes Schemmel, and Karlheinz Meie 2016. “Stochastic Inference with Spiking Neurons in the High-Conductance State.” Physi Review E 94 (4). https://doi.org/10.1103/PhysRevE.94.042312.

[10] Fiser, József, Pietro Berkes, Gergő Orbán, and Máté Lengyel. 2010. “Statistically Optimal Perception and Learning: From Behavior to Neural Representations.” Trends in Cognitive Sciences 14 (3): 119–30. https://doi.org/10.1016/j.tics.2010.01.003.

[11] Aitchison, Laurence, and Máté Lengyel. 2017. “With or without You: Predictive Coding a Bayesian Inference in the Brain.” Current Opinion in Neurobiology 46: 219–27. https://doi.org/10.1016/j.conb.2017.08.010.

[12] Probst, Dimitri, Mihai A. Petrovici, Ilja Bytschok, Johannes Bill, Dejan Pecevski, Johannes Schemmel, and Karlheinz Meier. 2015. “Probabilistic Inference in Discrete Spaces Can B Implemented into Networks of LIF Neurons.” Frontiers in Computational Neuroscience 9 (JAN): 1–11. https://doi.org/10.3389/fncom.2015.00013.

[13] Kungl, Akos F., Sebastian Schmitt, Johann Klähn, Paul Müller, Andreas Baumbach, Domir Dold, Alexander Kugele, et al. 2019. “Accelerated Physical Emulation of Bayesian Inferer in Spiking Neural Networks.” Frontiers in Neuroscience 13 (November). https://doi.org/10.3389/fnins.2019.01201.

[14] Neftci, Emre, Srinjoy Das, Bruno Pedroni, Kenneth Kreutz-Delgado, and Gert Cauwenberghs. 2014. “Event-Driven Contrastive Divergence for Spiking Neuromorphic Systems.” Frontiers in Neuroscience 7 (8 JAN). https://doi.org/10.3389/fnins.2013.0027

[15] Oliver Breitwieser, Andreas Baumbach, Agnes Korcsak-Gorzo, Johann Klähn, Max Brixne & Mihai Petrovici. (2020, February 24). sbs: Spike-based Sampling (v1.8.2) (Version v1.8. Zenodo. http://doi.org/10.5281/zenodo.3686015

[16] Gewaltig, Marc-Oliver, and Markus Diesmann. 2007. "NEST (NEural Simulation Tool)." Scholarpedia 2 (4): 1430. http://www.scholarpedia.org/article/NEST_(NEural_Simulation_Tool).

[17] Dold, Dominik, Ilja Bytschok, Akos F. Kungl, Andreas Baumbach, Oliver Breitwieser, Walt Senn, Johannes Schemmel, Karlheinz Meier, and Mihai A. Petrovici. 2019. "Stochasticity from Function — Why the Bayesian Brain May Need No Noise." Neural Networks 119 (November): 200–213. https://doi.org/10.1016/j.neunet.2019.08.002.

[18] Czischek, Stefanie, Andreas Baumbach, Sebastian Billaudelle, Benjamin Cramer, Lukas Kades, Jan M. Pawlowski, Markus K. Oberthaler, et al. 2020. "Spiking Neuromorphic Chi Learns Entangled Quantum States." http://arxiv.org/abs/2008.01039.

[19] Billaudelle, S., Y. Stradmann, K. Schreiber, B. Cramer, A. Baumbach, D. Dold, J. Goltz, et a 2020. "Versatile Emulation of Spiking Neural Networks on an Accelerated Neuromorphi Substrate," 1–1. https://doi.org/10.1109/iscas45731.2020.9180960.

Modelling cerebellar nuclei and NucleoCortical pathways

Massimo Grillo[1]*, Alice Geminiani[1,2], Alberto Antonietti[1,2], Egidio D'Angelo[2,3], Alessandra Pedrocchi[1]

[1] NEARLab, Department of Electronics, Information and Bioengineering, Politecnico di Milano, Milan, Italy
[2] Department of Brain and Behavioral Sciences, University of Pavia, Pavia, Italy
[3] IRCCS Mondino Foundation, Pavia, Italy
*massimo.grillo@polimi.it

INTRODUCTION/MOTIVATION

The cerebellum is a subcortical structure, whose main role in motor control is learning and coordination [1]. From an anatomical point of view, it can be subdivided into two major layers: cortex and deep nuclei. The cerebellar cortex processes input sensorimotor information and then, conveys signals toward the Deep Cerebellar Nuclei (DCN), which constitute the sole output stage of the cerebellum [2]. However, the information does not flow only from the cerebellar cortex to the cerebellar nuclei, since it was found that some DCN neurons project back to the cerebellar cortex, forming the so called NucleoCortical (NC) pathways [3]–[5].
In order to investigate the behaviour of DCN neurons during the execution of sensorimotor tasks, in-silico models of the cerebellum are often exploited. Available models of the cerebellar circuit include Spiking Neural Networks, inspired to anatomical and functional features of mouse cerebellum, such as: cells morphologies, anatomical connections, and electrophysiological behaviour of neurons and synapses [6], [7]. The most recent models of the DCN include only 2 out of 6 neuron types identified in literature [8] and projections from the input stage of the cerebellum towards the nuclei, without any backward connection (NC pathways). Since a detailed implementation of the cerebellar nuclei is crucial when simulating complex sensorimotor tasks, the aim of this work was to update the current in-silico DCN layer by including the NC pathways, which required the implementation of a new neural population in the DCN layer: the Glycinergic-Inactive (Gly-I) neurons.

METHODS

In order to replicate the functional behaviour of neurons inside an in-silico model, Spiking Neural Networks can be exploited. Recently, the neural simulator NEST has been developed within the Human Brain project and it represents a shared platform for Brain simulation [9]. For our purpose, the electroresponsive properties of Gly-I neurons were replicated through a single-point neuron model, the Extended-Generalized Leaky Integrate and Fire (E-GLIF) model [10], [11]. This model can reproduce complex electrophysiological behaviours with limited computational cost, thanks to a system of ordinary differential equations, which describe the dynamics of membrane potential and two intrinsic currents of the neuron. The model includes some electrophysiological parameters, extracted from literature, and other optimizable parameters, tuned through an optimization algorithm implemented in Matlab. Specifically, in order to implement Gly-I neurons, before running the optimization algorithm, a specific stimulation protocol with current steps was designed, allowing to evaluate their main electroresponsive features: no autorhythm, linear current-frequency relationship and high spike frequency adaptation [12]. After that, several optimizations were launched in order to find the best set of parameters which minimized the difference between the desired spike times and the actual times at which the E-GLIF membrane potential reached threshold; this way, the target firing rates for the different input current values in the stimulation protocol were fitted. Finally, the parameters were verified with NEST through single-neurons

simulations, in which one Gly-I neuron was stimulated with the same protocol used during optimization and its firing rates were computed after the stimulation onset (instantaneous firing rate) and near the end of each stimulation step (Steady-State firing rate).
At this point, by exploiting the cerebellar scaffold tool (https://github.com/dbbs-lab/bsb) [6], [7], [13], Gly-I neurons have been placed inside the DCN layer scaffold model, by defining the layer position, neuron density, and morphological properties. Considering the convergence and divergence ratios, they have been connected to other neurons inside the scaffold: Purkinje Cells and Mossy fibers, pre-synaptic neurons that provide inhibitory and excitatory inputs respectively [8], but also Golgi cells (GoCs) inside the cerebellar cortex, post-synaptic population inhibited by the activity of Gly-I neurons [4]. The synaptic parameters of the NC pathway were set considering that a Gly-I burst lasting around 50 ms caused a suppression in 25% of GoCs [4].

RESULTS AND DISCUSSION

In Figure 1, we can notice the behaviour of Gly-I model at rest and when stimulated by depolarizing current with increasing amplitude.

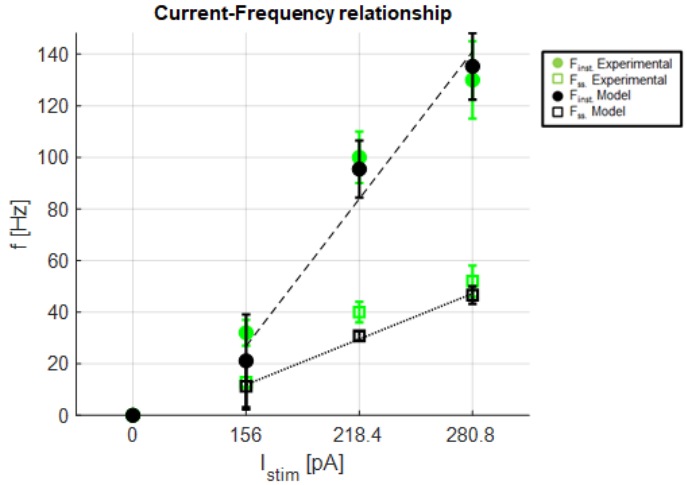

Figure 1: Current-Frequency relationship of Gly-I neuron during NEST simulations in two conditions: rest and depolarized by currents with increasing amplitude. Both instantaneous (dots) and Steady-State (squares) firing rates have been reported considering their average value among 50 simulations along with their standard deviation. Black symbols refer to model outcomes, whereas green symbols represent the experimental behaviour. The model values have been linearly interpolated (black lines).

At rest, no spiking activity was generated, while, when depolarized, the instantaneous firing rate increased almost linearly from around 20 Hz to 135 Hz. We can also notice that the Steady-State firing rate is much lower than the instantaneous firing rate, showing a high spike frequency adaptation: the firing rate strongly decreases from stimulation onset to the end of stimulation phase.
After the implementation of these neurons as E-GLIF models, they have been placed inside the cerebellum scaffold and connected with other neurons. In particular, Gly-I neurons received input signals coming from Mossy fibers and Purkinje cells and projected outside the DCN layer toward the cerebellar cortex, reaching 25% of GoCs, see Figure 2.A. The synaptic strength of the NC pathway made by Gly-I neurons has been properly tuned in order to replicate the suppression effect on GoCs: the population firing rate of GoCs decreases from 8.52 ± 0.82 Hz to 1.30 ± 0.71 Hz, see Figure 2.B.

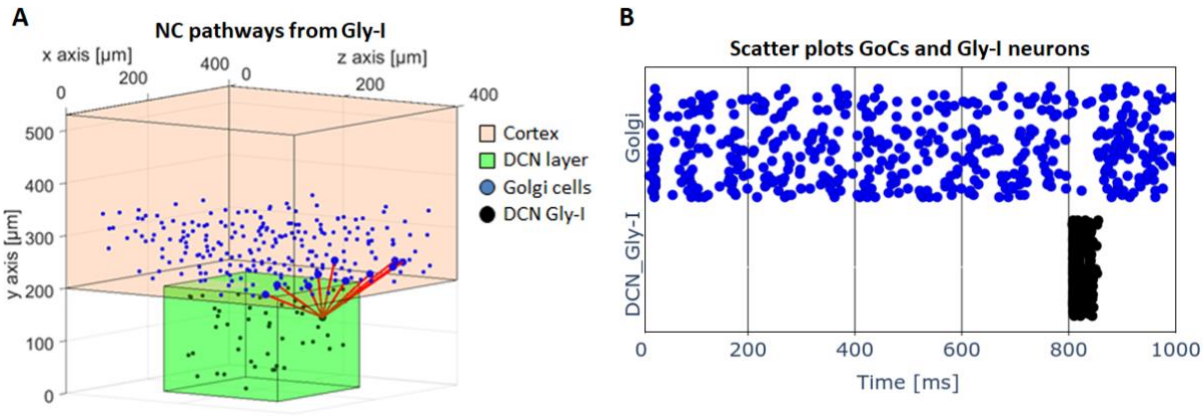

Figure 2: (A) Representation of the cerebellar cortex (pink), DCN layer (green) and NC pathways (redlines) connecting one Gly-I neuron (black dot) to several GoCs (blue dots) in the cerebellar cortex. (B) Scatter plots of GoCs and Gly-I neurons, showing the inhibitory effect of a glycinergic burst on GoCs activity.

To sum up, we here enhanced previous models of the cerebellar DCN layer adding a new neural population that projects back to the cerebellar cortex. The model will be exploited for more accurate simulations of complex cerebellum-driven tasks, where integration of input sensorimotor signals and cerebellar output feedback occurring in the cerebellar cortex is supposed to play a key role [5][14]. In addition, following the experimental characterization of the other neuron types in the DCN, the model will be further updated.

Keywords: Computational Neuroscience, Spiking Neural Networks, Cerebellum, NucleoCortical pathways

REFERENCES

[1] S. G. Lisberger, "The neural basis for learning of simple motor skills," *Science (80-.).*, 1988.

[2] J. F. Medina, W. L. Nores, T. Ohyama, and M. D. Mauk, "Mechanisms of cerebellar learning suggested by eyelid conditioning," *Current Opinion in Neurobiology*. 2000.

[3] B. D. Houck and A. L. Person, "Cerebellar loops: A review of the nucleocortical pathway," *Cerebellum*. 2014.

[4] L. Ankri *et al.*, "A novel inhibitory nucleo-cortical circuit controls cerebellar Golgi cell activity," *Elife*, 2015.

[5] Z. Gao *et al.*, "Excitatory Cerebellar Nucleocortical Circuit Provides Internal Amplification during Associative Conditioning," *Neuron*, 2016.

[6] A. Geminiani, A. Pedrocchi, E. D'Angelo, and C. Casellato, "Response Dynamics in an Olivocerebellar Spiking Neural Network With Non-linear Neuron Properties," *Front. Comput. Neurosci.*, 2019.

[7] S. Casali, E. Marenzi, C. Medini, C. Casellato, and E. D'Angelo, "Reconstruction and simulation of a scaffold model of the cerebellar network," *Front. Neuroinform.*, 2019.

[8] M. Uusisaari and T. Knöpfel, "Functional classification of neurons in the mouse lateral Cerebellar Nuclei," *Cerebellum*, 2011.

[9] J. M. Eppler, M. Helias, E. Muller, M. Diesmann, and M. O. Gewaltig, "PyNEST: A convenient interface to the NEST simulator," *Front. Neuroinform.*, 2009.

[10] A. Geminiani, C. Casellato, F. Locatelli, F. Prestori, A. Pedrocchi, and E. D'Angelo, "Complex dynamics in simplified neuronal models: Reproducing golgi cell

electroresponsiveness," *Front. Neuroinform.*, 2018.
[11] A. Geminiani, C. Casellato, E. D'Angelo, and A. Pedrocchi, "Complex electroresponsive dynamics in olivocerebellar neurons represented with extended-generalized leaky integrate and fire models," *Front. Comput. Neurosci.*, 2019.
[12] M. Uusisaari and T. Knöpfel, "GlyT2+ neurons in the lateral cerebellar nucleus," *Cerebellum*, 2010.
[13] R. De Schepper *et al.*, "The Brain Scaffold Builder, a package for structural and functional modelling of brain circuits: the cerebellar use case."
[14] B. D. Houck and A. L. Person, "Cerebellar premotor output neurons collateralize to innervate the cerebellar cortex," *J. Comp. Neurol.*, 2015.

Cerebro-cerebellar interactions: *in vivo* and *in silico* tools co-design

Francesco Jamal Sheiban[1], Alessandra Maria Trapani[1], Alice Geminiani[1,2], Egidio Ugo D'Angelo[2,3], Alessandra Pedrocchi[1]

[1] NEARLab, Department of Electronics, Information and Bioengineering, Politecnico di Milano, Milan, Italy;
[2] Department of Brain and Behavioural Sciences, University of Pavia, Pavia, Italy;
[3] IRCCS Mondino Foundation, Pavia, Italy.

INTRODUCTION

A major goal of contemporary neuroscientific research is to design experimental protocols for animal studies coupled with *in vivo* neural recordings to gather data so to investigate the brain mechanisms underlying behaviour [1]. Moreover, replicating those experiments *in silico* lets researchers develop and test computational models of the different brain areas involved and validate them against collected data. By faithfully reproducing biological features, such models can be used to test and/or suggest neurophysiological/pathological hypotheses and be eventually translated to clinical scenarios [1].

Recent findings ascribe cognitive functions to the cerebellum [2] that might be linked to cerebro-cerebellar interactions, though experimental tools and complementary computational models that investigate these connections in an exhaustive way are missing in literature [3]. The aim of this study is therefore the co-design of *in vivo* and *in silico* behavioural protocols and tools to be eventually used to investigate the functional role of cerebro-cerebellar interactions in motor learning tasks.

METHODS

Following this approach, the work presented here involves: (i) the implementation of a custom experimental setup for "reach-to-grasp" *in vivo* experiments on adult mice; (ii) the design of a neurorobotic setup to replicate the protocol *in silico*, including a virtual environment and a robotic subject embodying a functional spiking neural network; (iii) the simulation of a behavioural task execution using the neurorobot.

The target behavioural protocol of this study is a "reach-to-grasp" movement to collect water droplets at two possible locations, marked by an anticipatory directional (left/right) cue. For the *in vivo* experimental procedure, water deprived mice are trained to reach the reward after a time-varying delayed go-cue (i.e., a sound) from a fixed starting point, by associating the direction of an early stimulus to the reward location.

Thus, a sensorized cage was designed to house animal during the task execution and automatically deliver the protocol stimuli with precise timings via integrated sensors and actuators. The overall system was controlled by an Arduino ® Mega 2560 board communicating with a user-friendly graphical interface designed for setting protocol parameters and monitoring task execution in real-time.

Along with the implementation of the *in vivo* apparatus, the behavioural protocol was reconstructed on the NeuroRobotics Platform (NRP) [4]. The *in silico* task was designed to closely mimic its *in vivo* counterpart by employing the iCub humanoid robot and providing the same environmental stimuli via custom-designed transfer functions.

This virtual implementation also required the design of a brain network model of integrate-and-fire neurons driving the neurorobot movements, with constant synaptic weights tuned via a trial-and-error procedure. The reconstructed model, designed following biological

findings, included two identical modules (to discriminate the directional stimuli) and feedback loops between premotor and frontal cortices [5][6], motor thalamus [7][8] and cerebellum [9] to reproduce short-term memory and temporal decisions mechanisms. More specifically, cortical areas consisted of the medial prefrontal cortex (mPFC), the secondary (ALM) and primary (CFA, RFA) motor cortex and the primary somatosensory cortex (vS1) regions. The thalamic areas comprised nuclei from the ventral lateral (VL, VAL) and posterior (VPM) regions (Figure 1).

RESULTS AND DISCUSSION

As a result of the *in vivo* and *in silico* co-design, we released and tested the first prototype of the experimental set-up, adjusting the components design to adapt it to real-case scenarios and completing the hardware circuitry along with the real-time communication between the software and the micro-controller. Then, the entire experimental protocol was correctly executed *in silico* by the neurorobot using a scaled-down neural network of the designed brain model (Figure 1).

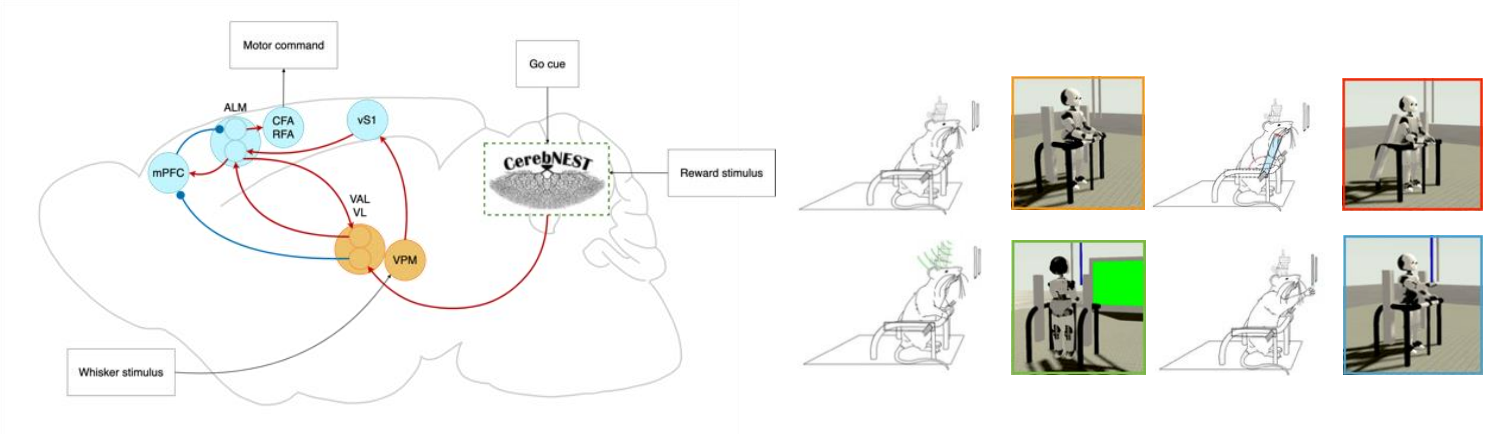

Figure 1: In vivo and in silico protocols co-execution. The iCub robot, when provided with a SNN composed of two identical modules, whose structure is schematically reported in the figure [left], successfully performed the behavioural task as it was designed to be executed in vivo [right]. The virtual subject waited in standing position with its hand on a fixed starting point (orange box), receiving a somatosensory stimulus on its shoulder (red box) simulating the in vivo directional stimulus (a whisker touch). Then, the robot waited motionless until a go-cue (green box) signalled reward availability, upon which it performed the grasping movement (blue box) mirroring the somatosensory stimulus direction.

Concerning the *in silico* protocol reconstruction, we managed to provide the same *in vivo* experimental stimuli to the neurorobot, implementing different transfer functions to carry signals from the environmental and robotic sensors to the spiking neural network.

Monitoring the activity of the tuned spiking neural network, we evaluated the capability of reproduce spiking responses supposed to occur at the beginning and end of cerebellum-driven learning. Specifically, we assessed that the premotor cortex/thalamus loop, the medial prefrontal cortex and the motor cortex were able to sustain preparatory activity, block impulsive actions and drive movement execution, respectively, once provided with the expected cerebellar activity at the end of learning, as opposed to being disconnected from the cerebellar module (Figure 2).

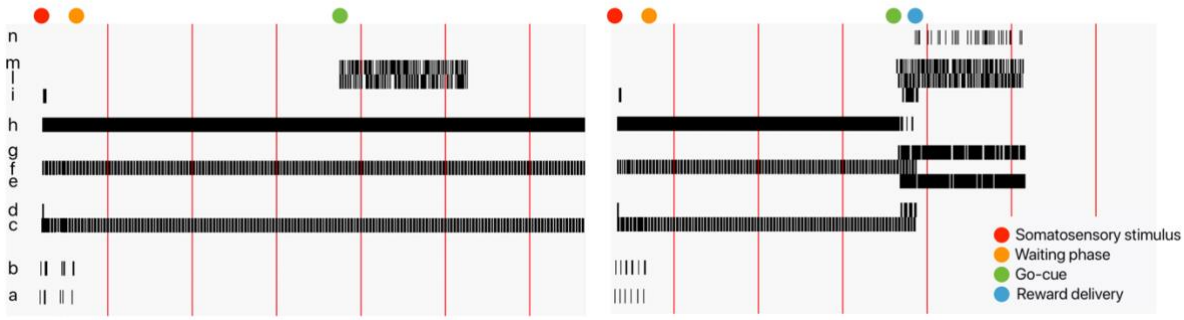

Figure 2: Sensorimotor signals encoding in the network. The spike activity recorded without [left] and with [right] the supposed post-learning cerebellar input dynamics to the cerebral nodes. Without these inputs, the ALM/VL-VLA loop (c-f) and mPFC area (h) are not silenced upon go-cue exhibition (l-m), thus their sustained activity persists after the screen is set to green. Conversely, with the proper cortico-cerebellar connections, the go signals cause the inhibitory VL-VLA areas (e-g) to stop the mPFC and subsequent ALM-premotor (d) and CFA-RFA (i) activation drives the neurorobot in correctly performing the movement.

These results represent a solid basis on which to continue the co-design of in vivo and in silico protocols, improving the prototype of the experimental set-up, acquiring animal data, refining the neural network model (e.g., scaling up the network and embedding distributed plasticity) and simulating the full learning protocol, eventually exploiting high-performance computing resources.

Acknowledgments: This work is supported by CerebNEST and RisingNet projects within the European Union's Horizon 2020 Framework Programme for Research and Innovation under the Specific Grant Agreement No. 945539 (Human Brain Project SGA3). We thank Ileana Montagna, PhD, Department of Brain and Behavioral Sciences, University of Pavia, for the experimental setup design support.

REFERENCES

[1] J. N. Crawley and A. Holmes, "Behavioral Neuroscience," Current Protocols in Neuroscience, no. April, pp. 1–2, 2011.

[2] E. D. Angelo and S. Casali, "Seeking a unified framework for cerebellar function and dysfunction : from circuit operations to cognition," Frontiers in Neural Circuits, vol. 6, no. January, pp. 1–23, 2013.

[3] M. J. Wagner and L. Luo, "Neocortex – Cerebellum Circuits for Cognitive Processing," Trends in Neurosciences, vol. 43, no. 1, pp. 42–54, 2020.

[4] E. Falotico, L. Vannucci, A. Ambrosano, and U. Albanese, "Connecting Artificial Brains to Robots in a Comprehensive Simulation Framework: The Neurorobotics Platform," Frontiers in Neurorobotics, vol. 11, no. January, pp. 1–19, 2017.

[5] A. Saiki, R. Kimura, T. Samura, Y. Fujiwara-Tsukamoto, and Y. Sakai, "Different Modulation of Common Motor Information in Rat Primary and Secondary Motor Cortices," PLOS ONE, vol. 9, no. 6, pp. 1–13, 2014.

[6] M. Murakami, H. Shteingart, Y. Loewenstein, Z. F. Mainen, "Distinct Sources of Deterministic and Stochastic Components of Action Timing Decisions in Rodent Frontal Cortex," Neuron, vol. 94, no. 4, pp. 908–919., 2017.

[7] Z. V. Guo, H. K. Inagaki, K. Daie, S. Druckmann, C. R. Gerfen, and K. Svoboda, "Maintenance of persistent activity in a frontal thalamocortical loop," Nature, 2017.

[8] N. Sakayori, S. Kato, M. Sugawara, S. Setogawa, H. Fukushima, R. Ishikawa, S. Kida, and K. Kobayashi, "Motor skills mediated through cerebellothalamic tracts projecting to the central lateral nucleus," Molecular Brain, pp. 1–12, 2019

[9] F. P. Chabrol, A. Blot, T. D. Mrsic-Flogel, "Cerebellar Contribution to Preparatory Activity in Motor Neocortex," Neuron, vol. 103, no. 3, pp. 506–519, 2019.

Modelling neural dynamics on neuromorphic hardware

Mollie Ward[1]*, Oliver Rhodes[1]

[1] Department of Computer Science, University of Manchester, Manchester, UK
*Correspondence: mollie.ward@manchester.ac.uk

INTRODUCTION AND MOTIVATION

Accurate and efficient simulation of neural activity has long been a goal in computational neuroscience research. Neuromorphic computing aims to provide platforms for energy-efficient exploration of computational neuroscience through simulation of Spiking Neural Networks (SNNs): networks of individual neuron models designed to mimic biological networks[1,2]. These SNNs generally incorporate a simple model called the Leaky Integrate-and-Fire (LIF) model[3] which simplifies a number of biological features resulting in the loss of a range of neuronal characteristics including the ability to compute operations such as XOR. Incorporation of more biologically accurate dynamics onto neuromorphic systems could be therefore be fundamental to further understanding of the brain.

LIF neurons are modelled as point processes with a single term describing membrane conductance. In reality, neurons are not this simple and more complex models exist describing these simplified features: ion-channels governing membrane conductance can be described using mathematical approximations, and the cable equation captures complex, elongated structures incorporating branched dendritic extensions[3] through multi-compartment models[4,5] (Figure 1).

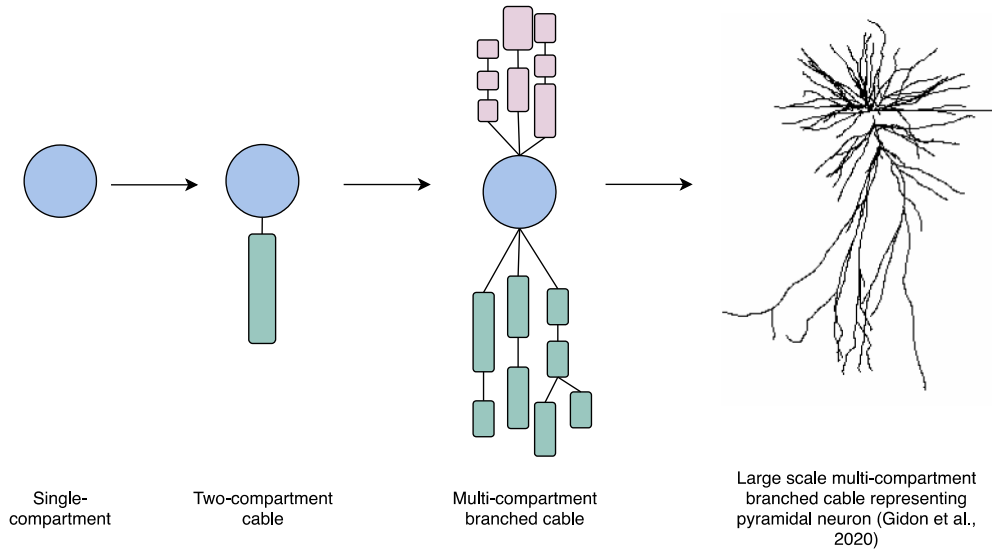

Figure 1: Neuron models increasing in complexity. Neurons are approximated as a number of compartments, each described by a single membrane potential. The simplest model is a single compartment model e.g. LIF model. Detailed neuronal morphologies can be captured with multicompartment models e.g. Gidon et al.[5] 's pyramidal cell (far right).

However, increasing the complexity of models increases computational costs; large-scale simulations of SNNs with complex neuron models[4], while effective, consume megawatts of power simulating small regions of the brain (0.29 mm^3)[4,6]. This is not mimicked in the brain which demonstrates a remarkable ability for large amounts of fine-scale computation at a fraction of the power (up to 20 Watts), much faster than these SNNs[1,7]. Neuromorphic systems

provide a potential solution by mimicking the brain, enabling real-time simulations by using processors which are less complex than those used in standard computing platforms[1,8]. However, use of these processers limits the complexity of modelling available; some platforms have energy-efficient hard-coded circuitry, limiting flexibility of trialling new models. Implementation of complex models is therefore a challenge as mathematical operations such as exponentials and divides are not often available yet feature heavily in the models.
Here, the advantages and challenges of implementing more biologically realistic models on neuromorphic hardware while aiming to maintain energy-efficiency are explored. Requirements for accurate and efficient ion-channel modelling are demonstrated with an example of how these dynamics can be incorporated into a multi-compartment model, giving single neurons XOR-solving properties never before demonstrated on neuromorphic hardware.

METHODS

The SpiNNaker neuromorphic platform[9] is used due to its software programmable nature and flexibility, enabling exploration of different neural models incorporating operations such as exponentials and divisions.

The basic equation for all single-compartment neurons includes a term, i_m, describing the current per unit area ($\mathrm{nA/mm^2}$). In Integrate-and-Fire models, i_m consists of a single passive leakage term which can be expanded to include ion-channel conductances in more complex models, described by calculating the current conducted by the channel:

$$i_m = \bar{g}P(V - E)$$

Where $\bar{g}$ is the single channel open conductance per unit area ($\mathrm{mS/mm^2}$), P is the probability that the channel is open and E is the reversal potential (mV). Potassium and sodium channel currents are modelled as $\bar{g}_K n^4(V - E_K)$ and $\bar{g}_{Na} m^3 h(V - E_{Na})$ where n and m are activation parameters for each channel respectively; sodium channels also have an inactivation parameter, h. These conductances were originally described by Hodgkin and Huxley[10] and are here modelled on SpiNNaker[9] with testing in voltage-clamping experiments and comparison with a reference floating-point Python implementation.

A two-compartment reference model is built based on the multi-compartment neuron model described by Gidon et al. 2020[5]. This model is constructed in the NEURON simulator, along with a version in Python to explore accuracy and performance. The soma incorporates sodium (I_{Na}) and potassium (I_K) currents and the dendrite features a calcium (I_{Ca}) current responsible for dendritic calcium action potentials (dCaAPs) when the membrane potential crosses -36 mV. Membrane potential in each compartment, μ, is governed by the cable equation:

$$c_m \frac{dV_\mu}{dt} = -i_m + \frac{I_e^\mu}{A_\mu} + g_{\mu,\mu\pm1}(V_{\mu\pm1} - V_\mu)$$

Where c_m is the specific membrane capacitance ($\mathrm{nF/mm^2}$), I_e^μ is the electrode current (nA), $A_\mu$is the total surface area ($\mathrm{mm^2}$) and $g_{\mu,\mu\pm1}$ is internal coupling conductance ($\mathrm{nS/mm^2}$).

RESULTS AND DISCUSSION

Despite additional mathematical complexity, SpiNNaker[9] is able to accurately model the potassium and sodium channel conductances. Terms m, n and h are described by differential

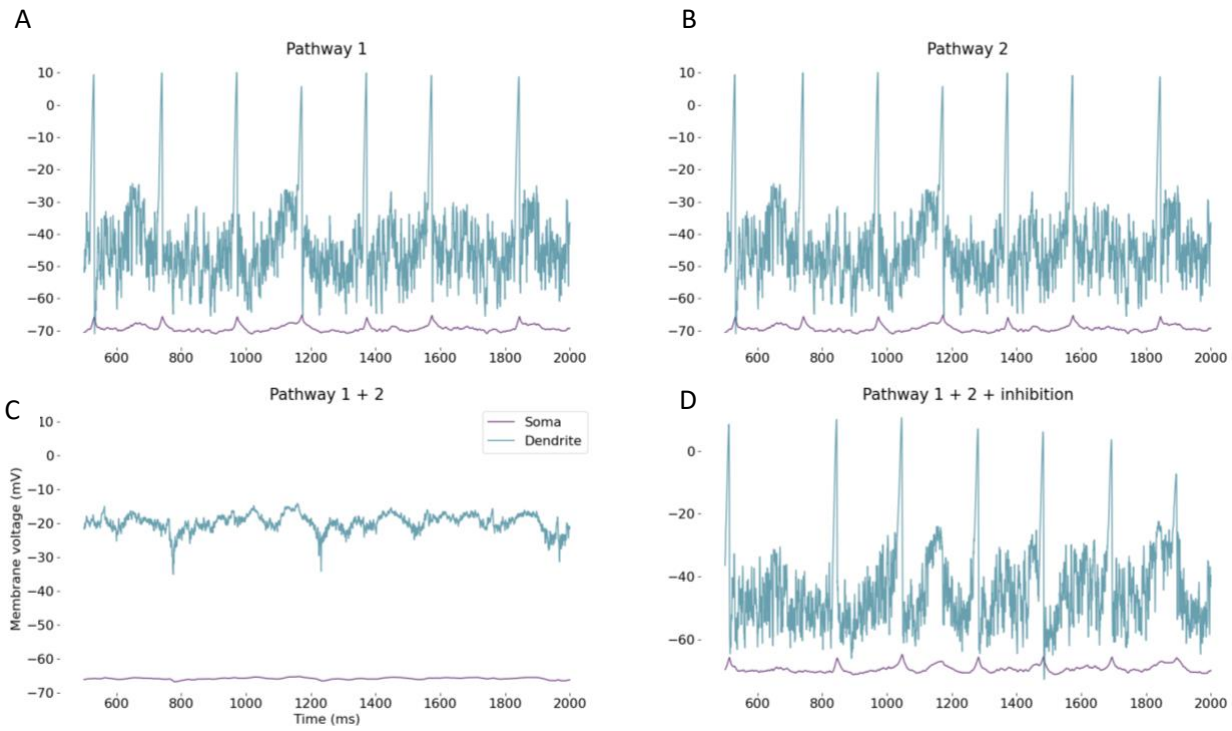

Figure 2: Two compartment dendrite-soma model in NEURON[9] environment demonstrating XOR properties. (A) Stimulation of a single pathway with 15 excitatory synaptic connections results in the dendritic compartment firing dCaAPs. (B) As (A) with separate, identical pathway. (C) Stimulation of both pathways results in the loss of dCaAPs. (D) dCaAPs restored when both pathways are stimulated with 15 inhibitory synapses.

equations and solving them requires a number of calculations including divisions and an exponential. Simplifying assumptions which give a biologically faithful model were sought, including treating variables exhibiting small changes as constant, enabling pre-calculation of certain costly operations and removing three sets of exponential and divide operators.

The two-compartment model under exploration contains a variety of these ion-channel conductances and hence illustrates an example of the dynamic properties a neuron can exhibit when incorporating conductances. The model contains a dendritic compartment with XOR-solving capabilities (Figure 2; A-D). The calcium-channel current suppresses the amplitude of action potentials when the input strength is increased above a threshold, giving capabilities to a single neuron which would previously have required a network solution.

FUTURE WORK

The two-compartment model built in NEURON[11] and Python will be implemented on SpiNNaker[9] and efforts made to improve efficiency; the feasibility of using a lookup table to pre-calculate certain voltage-dependent operations involved in the calculation of activation parameters is under investigation which will significantly increase the efficiency of the models described.

Addition of these dynamics onto neuromorphic hardware will enable replication of a wide range of neuronal firing characteristics observed in biology; efficient and accurate implementation of these models are therefore of interest to both computational neuroscience and AI communities.

REFERENCES

1. Roy, K., Jaiswal, A. & Panda, P. Towards spike-based machine intelligence with neuromorphic computing. *Nature* **575**, 607–617 (2019).
2. Furber, S. Large-scale neuromorphic computing systems. *J. Neural Eng.* **13**, (2016).
3. Dayan, P. & Abbott, L. F. *Theoretical Neuroscience: Computational and Mathematical Modeling of Neural Systems*. (The MIT Press, 2005).
4. Markram, H. *et al.* Reconstruction and Simulation of Neocortical Microcircuitry. *Cell* **163**, 456–492 (2015).
5. Gidon, A. *et al.* Dendritic action potentials and computation in human layer 2/3 cortical neurons. *Science (80-.).* **367**, 83–87 (2020).
6. Wallace, S., Vishwanath, V., Coghlan, S., Lan, Z. & Papka, M. E. Measuring power consumption on IBM Blue Gene/Q. *Proc. - IEEE 27th Int. Parallel Distrib. Process. Symp. Work. PhD Forum, IPDPSW 2013* 853–859 (2013). doi:10.1109/IPDPSW.2013.269
7. Cox, D. D. & Dean, T. Neural networks and neuroscience-inspired computer vision. *Curr. Biol.* **24**, R921–R929 (2014).
8. Rhodes, O. *et al.* Real-time cortical simulation on neuromorphic hardware. *Philos. Trans. R. Soc. A Math. Phys. Eng. Sci.* **378**, (2020).
9. Furber, S. B., Galluppi, F., Temple, S. & Plana, L. A. The SpiNNaker project. *Proc. IEEE* **102**, 652–665 (2014).
10. Hodgkin, A. L. & Huxley, A. F. A quantitative description of membrane current and its application to conduction and excitation in nerve. *J. Physiol* **117**, (1952).
11. Hines, M. L. & Carnevale, N. T. The NEURON Simulation Environment. *Neural Comput.* **9**, 1179–1209 (1997).

IV Cognitive and behavioral neuroscience

How affective looming sounds modulate the whole-body action preparation within peripersonal space: the case of stepping congruent/incongruent to affect

Mehrdad Bahadori[1]*, Paola Cesari[1]

[1] Department of Neuroscience, Biomedicine, and Movement Sciences, University of Verona, Verona, Italy
*Mehrdad.bahadori@univr.it

INTRODUCTION/MOTIVATION

The peripersonal space (PPS) has found to have specific sensory-motor representation in the brain. Previous literature has dedicated two functions to sensory-motor behavior within PPS: a rapid sensory-motor interface for defensive purpose, and a sensory-motor interface serving goal-directed actions [1]. In this study, we investigate how the different affective (positive, negative, and neutral) looming sounds (approaching either from left or right) stopping at different distances (close and far) within the PPS, modulate action preparation in a whole-body movement as stepping. We were expecting that action preparation strategies were following motivational direction; e.g. stepping faster toward (away from) a positive (negative) approaching sound. To measure action preparation as a reflection of a feed-forward command from the motor cortex, force, and electromyographic premotor reaction times (PRTs) have been measured [2]. Additionally, step width, step duration, and maximum velocity have been registered by recording kinematics via motion capture.

METHODS

Sixteen right leg dominant participants have participated in the experiment. Emotional sounds were selected from the IADS dataset having different levels of induced valence and arousal. Five positive and five negative sounds have been selected from the IADS database [3]. As neutral sound, different colors of noises (5 sounds: red, pink, white, blue, and violet noise) were selected [4]. The sounds were modulated in a way that they were approaching either from the left (-80°) or the right (80°) side with zero degrees of elevation from the ear canal filtered by using KEMAR HRTF provided by CIPIC dataset [5]. Participants were standing barefoot putting each foot on one of the two side-by-side force plates. The two different experimental conditions for action were defined based on the stepping direction according to the approaching sound direction: 1) stepping toward the approaching sound 2) stepping away from the approaching sound. The force premotor reaction time (FPRT) and electromyography premotor reaction time data (EPRT) considering Tibialis Anterior (TA), Adductor (AD), Rector Femoris (RF), and Gluteus Medius (GM), have been registered, along with kinematics data. The FPRT was defined as the time difference between the sound offset and the onset of force changes, while the EPRT for each muscle have been defined as the time difference between the sound offset and the onset of the muscle activity (considering the standing leg) (Figure 1). For statistical analysis, a separate repeated measures ANOVA was deployed for each variable by considering Action (toward/away) × Emotion (positive/negative/neutral) × Distance (close/far) as within-subjects variables.

RESULTS AND DISCUSSION

The results revealed prompter step while reacting to closer sounds compared to further sounds, regardless of the emotional content of the sounds and Action (Figure 2). This result is in line with previous studies, which show the enhanced motor cortex activation while an external stimulus is very close to the body [6, 7]. Furthermore, our results showed that the PRTs were being modulated by the emotional content of the sound. The results showed that FPRT (Figure 2) and EPRT in all anticipatory muscles was shorter while reacting to neutral sounds compared to both positive and negative sounds, which might be due to lower perceptual load given the simpler sound composition in terms of frequency components [8]. Interestingly, FPRT and EPRT of GM muscle in standing leg for negative sound was shorter than positive sound. Previous studies suggest that, while emotions are closely linked to actions, negative events require more prompt reactions and need to be more crucially prepared [9].

Importantly, the results revealed shorter FPRTs and EPRTs in the far distance while reacting to negative sounds compared to positive sounds. Previous studies have concluded the expansion of PPS followed by negative emotions, by measuring different behavioral and neurophysiological variables [4, 10]. It is shown that time-to-collision underestimation is enhanced for individuals who are fearful of the threatening stimulus and the size of the underestimation is linked to individuals' level of threat-related anxiety [11, 12]. If PPS is extended, the distance between the feared object and PPS boundaries is smaller, consequently, the entrance within the PPS occurs sooner. Thus, the fact that an approaching negative stimulus is perceived as colliding sooner seems coherent with the PPS boundaries being farther. Concludingly, in line with the above-mentioned studies, the results showed that the whole-body PPS space is extended in presence of negative emotion which leads to promoter whole-body movement such as stepping.

Besides, the data revealed that the step width was larger when sounds were closer to the body compared to the far distances. Importantly, the post-hoc analysis showed that the step length did not change for positive sound in the close and far distance, but it was bigger for negative and neutral sounds in close distance compared to far distance. According to distance regulation hypothesize, the changes in the physical proximity of an actor to the outside world follows the approach and avoidance behavior [13]. Accordingly, since a stimulus within PPS triggers a flight behavior as well as an induced negative emotion by the stimuli, the steps were larger while reacting to a stimulus very close to the body or negative but not positive one.

In this experiment, the data did not show any significant difference in Action condition in none of the measured variables. However, we think that one of the reasons that we did not find any difference in Action is due to using sounds instead of images, since reactions to emotional images have found to be stronger [14] and more immediate [15] compared to sounds; thus our stimuli were not sufficient enough to drive stepping, which is a sophisticated motor task [16], in direction of approach and avoidance behavior.

To conclude, this study showed that the movement preparation of stepping, as a whole-body sophisticated movement, in presence of the external stimuli is modulated based on the distance of the stimuli within PPS and the affects induced by the stimuli. The results add new evidence about the role of PPS as a movement regulating factor and how affects induced by external stimuli modulate these multisensory-motor regulations within PPS.

Keywords: Peripersonal space, looming sound, emotion, reaction time, motivation

FIGURES

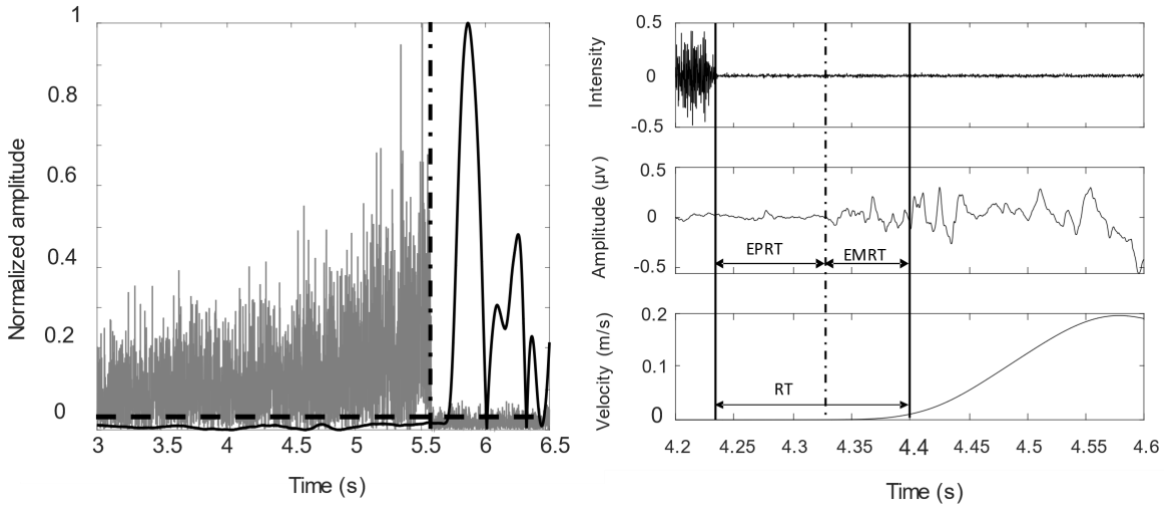

Figure 1 left) detecting force onset procedure in one trial, to calculate the FPRT by subtracting it from the offset of the sound. The grey signal is the normalized sound stimuli, the black signal is the normalized absolute value of the force, the vertical dash-dot line is the offset of the sound, and the horizontal dash line is the threshold of force initiation. The first sample in force signal exceeding the threshold after the sound offset is considered as the force onset. right) the variables calculated from EMG analysis. The graphs are showing the sound intensity, EMG activity of one muscle, and velocity of the moving leg in one trial from top to bottom respectively. The first and last solid vertical lines are showing the sound offset and kinematics onset respectively. The vertical dash-dot line shows the onset of EMG activity. The EPRT is the time between offset of the sound and onset of EMG activity, the EMRT it the time between onset of the muscle activity and onset of the kinematic, and the RT (Reaction Time) is the time between offset of the sound and the onset of the kinematics.

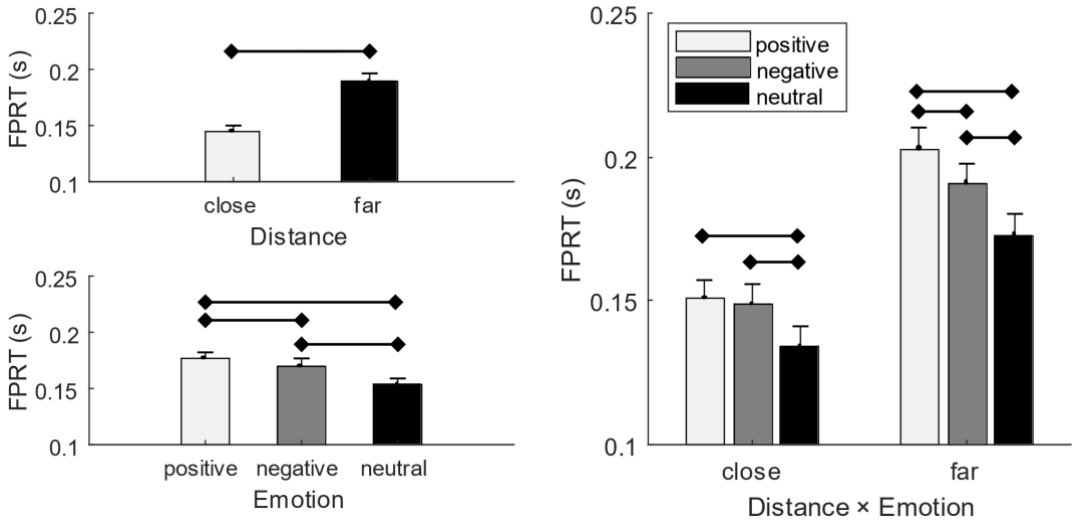

Figure 2 the FPRTs of standing leg for different Emotions (positive/negative/neutral) Distances (close/far) and their interactions. The error bars show the standard error and the black lines show a significant difference at the level of α<0.05.

REFERENCES

1. Rizzolatti, G., L. Fogassi, and V. Gallese, *Motor and cognitive functions of the ventral premotor cortex.* Current opinion in neurobiology, 2002. **12**(2): p. 149-154.
2. Santos, M.J., N. Kanekar, and A.S. Aruin, *The role of anticipatory postural adjustments in compensatory control of posture: 2. Biomechanical analysis.* Journal of Electromyography and Kinesiology, 2010. **20**(3): p. 398-405.
3. Bradley, M.M. and P.J. Lang, *The International Affective Digitized Sounds (; IADS-2): Affective ratings of sounds and instruction manual.* University of Florida, Gainesville, FL, Tech. Rep. B-3, 2007.
4. Ferri, F., et al., *Emotion-inducing approaching sounds shape the boundaries of multisensory peripersonal space.* Neuropsychologia, 2015. **70**: p. 468-475.
5. Algazi, V.R., et al. *The cipic hrtf database*. in *Proceedings of the 2001 IEEE Workshop on the Applications of Signal Processing to Audio and Acoustics (Cat. No. 01TH8575)*. 2001. IEEE.
6. Camponogara, I., N. Komeilipoor, and P. Cesari, *When distance matters: Perceptual bias and behavioral response for approaching sounds in peripersonal and extrapersonal space.* Neuroscience, 2015. **304**: p. 101-108.
7. Cléry, J., et al., *Neuronal bases of peripersonal and extrapersonal spaces, their plasticity and their dynamics: knowns and unknowns.* Neuropsychologia, 2015. **70**: p. 313-326.
8. Bahadori, M., et al., *Action planning and affective states within the auditory peripersonal space in normal hearing and cochlear-implanted listeners.* Neuropsychologia (under revision), 2020.
9. Borgomaneri, S., V. Gazzola, and A. Avenanti, *Temporal dynamics of motor cortex excitability during perception of natural emotional scenes.* Social cognitive and affective neuroscience, 2013. **9**(10): p. 1451-1457.
10. Ruggiero, G., et al., *The effect of facial expressions on peripersonal and interpersonal spaces.* Psychological research, 2017. **81**(6): p. 1232-1240.
11. Brendel, E., et al., *Threatening pictures induce shortened time-to-contact estimates.* Attention, Perception, & Psychophysics, 2012. **74**(5): p. 979-987.
12. Vagnoni, E., S.F. Lourenco, and M.R. Longo, *Threat modulates perception of looming visual stimuli.* Current biology, 2012. **22**(19): p. R826-R827.
13. Chen, M. and J.A. Bargh, *Consequences of automatic evaluation: Immediate behavioral predispositions to approach or avoid the stimulus.* Personality and social psychology bulletin, 1999. **25**(2): p. 215-224.
14. Bradley, M.M. and P.J. Lang, *Affective reactions to acoustic stimuli.* Psychophysiology, 2000. **37**(2): p. 204-215.
15. Thierry, G. and M.V. Roberts, *Event-related potential study of attention capture by affective sounds.* Neuroreport, 2007. **18**(3): p. 245-248.
16. Rocchi, L., et al., *Step initiation in Parkinson's disease: influence of initial stance conditions.* Neuroscience letters, 2006. **406**(1-2): p. 128-132.

Influence of perinatal maternal high fat diet on hedonic responding in adolescent offspring

Harshit Bhasin*, Matthew M. Hurley, Aliasgher Sabir, Shannon C. O'Brien, Timothy H. Moran, Kellie L. K. Tamashiro

The Johns Hopkins University School of Medicine, Department of Psychiatry & Behavioral Sciences, Baltimore, MD USA.
*hbhasin1@jhu.edu

INTRODUCTION/MOTIVATION

Studies have shown that male offspring of overweight parents are 1.7 times more likely to be overweight than the children of healthy parents (1). Maternal obesity has been shown to have an impact on the fetus and have an increased risk of obesity in the offspring (2-4). Previous studies show lowered dopamine sensitivity in obese individuals (5) which is thought to be, in part, responsible for the development of overeating behaviors. **The current experiment was designed to examine the impact of maternal diet on male offspring Sprague-Dawley rat innate reward valuation and the brain reward system.** This was done by measuring orofacial responding using the taste reactivity test (TRT) paradigm at two timepoints of the offspring's life. Briefly, the TRT involves analyzing orofacial responses that are conserved across species. Human infants, baby monkeys, and rodents have conserved responses that may be interpreted as "liking" or "disliking" (10,11). This allows us to assess the hedonic state of the animal by quantifying such orofacial responses by watching behavioral videos frame by frame. Previous studies showed that offspring of dams who consumed high fat (HF) diet during gestation and lactation are obese with impaired glucose tolerance and leptin resistance by the time they were weaned compared to standard chow (SC) offspring (6-7). We previously demonstrated that HF rat offspring have a greater preference for palatable food when given a choice. A Brief-Access Taste Test showed no differences between the groups in taste sensitivity (8). However, it is possible that HF offspring have altered 'liking' responding to palatable tastants and this is what drives them to consume more palatable food leading to obesity.

METHODS

Pregnant rats were placed on a Standard Chow ("SC"; n=6) or High-Fat diet ("HF"; n=6) beginning on gestation day (G)2. At weaning on postnatal day (P)21, male offspring (n=11 SC; n=16 HF) were selected from each litter and underwent surgery to implant intraoral catheters which was used to infuse tastants into the animal's mouth. The animals underwent an initial TRT with a 1M sucrose solution at P28-29. Behavior during the test was video recorded for later analysis. At P42, animals underwent a second taste reactivity test with a 1M sucrose solution after which the animals were sacrificed. Videos were scored by 3 scorers blind to the experimental conditions and individual 'liking' and 'disliking' responses were recorded. The scores from all 3 raters were averaged to account for human error.

RESULTS AND DISCUSSION

On P28 offspring were challenged with a 1 molar sucrose TRT. HF offspring displayed significantly fewer cumulative 'liking' responses, compared to the SC offspring (**Fig 1 TEST ONE).** When the animals were tested again on P42, HF offspring again displayed significantly less cumulative 'liking' responses compared to the SC offspring **(Fig 1 TEST TWO**)**.** Both groups

showed lower responding at P42 than at P28, in line with previous literature that 'liking' responses reduce with age (12). Taken together, we found that offspring of dams consuming a high fat diet during pregnancy display fewer orofacial responding to a sweet tastant, suggesting blunted hedonic responding. This supports our hypothesis that HF offspring may be driven to consume more palatable food due to an impaired hedonic state leading to obesity.

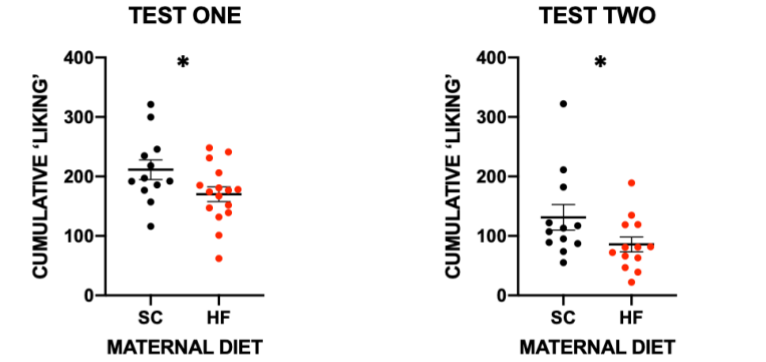

Fig 1: Cumulative liking responses from test one and test two

Keywords: Maternal Diet, Obesity, Taste Reactivity Test, Hedonic Responding

REFERENCES

[1] BAHREYNIAN, M., QORBANI, M., KHANIABADI, B. M., MOTLAGH, M. E., SAFARI, O., ASAYESH, H. & KELISHADI, R. 2017. Association between Obesity and Parental Weight Status in Children and Adolescents. *J Clin Res Pediatr Endocrinol,* 9**,** 111-117

[2] Yu, Z., et al., Trends in overweight and obesity among children and adolescents in China from 1981 to 2010: a meta-analysis. PLoS One, 2012. 7(12): p. e51949.

[3] Drake, A.J., et al., An unbalanced maternal diet in pregnancy associates with offspring epigenetic changes in genes controlling glucocorticoid action and foetal growth. Clin Endocrinol (Oxf), 2012. 77(6): p. 808-15.

[4] Drake, A.J. and R.M. Reynolds, Impact of maternal obesity on offspring obesity and cardiometabolic disease risk. Reproduction, 2010. 140(3): p. 387-98.

[5] Volkow N. D.; Wang G. J.; Fowler J. S.; Telang F. (2008) Overlapping neuronal circuits in addiction and obesity: Evidence of systems pathology. Philos. Trans. R. Soc., B 363, 3191–3200.

[6] Sun, B., et al., Maternal high-fat diet during gestation or suckling differentially affects offspring leptin sensitivity and obesity. Diabetes, 2012. Jun 29 [Epub ahead of print].

[7] Tamashiro, K.L., et al., Prenatal stress or high-fat diet increases susceptibility to diet-induced obesity in rat offspring. Diabetes, 2009. 58(5): p. 1116-25.

[8] Y. Treesukosol, B. Sun, A.A. Moghadam, N.C. Liang, K.L. Tamashiro, T.H. Moran. Maternal high-fat diet during pregnancy and lactation reduces the appetitive behavioral component in female offspring tested in a brief-access taste procedure Am. J. Physiol. Regul. Integr. Comp. Physiol., 306 (7) (2014), pp. R499-R509

[9] Grill HJ, Norgren R. The taste reactivity test. I. Mimetic responses to gustatory stimuli in neurologically normal rats. Brain Research. 1978;143(2):263-79

[10] Berridge, K.C. “Measuring Hedonic Impact in Animals and Infants: Microstructure of Affective Taste Reactivity Patterns.” *Neuroscience & Biobehavioral Reviews*, Pergamon, 17 Feb. 2000.

[11] Berridge, Kent C., and Morten L. Kringelbach. “Pleasure Systems in the Brain.” *Neuron*, Cell Press, 6 May 2015.

[12] Wilmouth, Carrie E, and Linda P Spear. “Hedonic sensitivity in adolescent and adult rats: taste reactivity and voluntary sucrose consumption.” Pharmacology, biochemistry, and behavior vol. 92,4 (2009): 566-73. doi:10.1016/j.pbb.2009.02.009

Deep-sleep-inspired activity induces density-based-clustering on memories and entropic, energetic and classification gains

Chiara De Luca[1,2]*, Cristiano Capone[1], Pier Stanislao Paolucci[1]

[1]Istituto Nazionale di Fisica Nucleare (INFN)
[2] PhD Behavioural Neuroscience, La Sapienza University
*Chiara.DeLuca@infn.roma1.it

INTRODUCTION/MOTIVATION

Sleep is known to be essential for awake performance[1][2], but the mechanisms underlying its cognitive functions are still to be clarified: here we aim to investigate the effect of deep-sleep like activity over internal memories representation. Relying on very minimal assumptions, which are the thalamo-cortical structure and the presence of cortically generated cortico-thalamic slow oscillations we formally find out that sleep might naturally perform a "density-based clustering" in the thalamo-cortical connections. We demonstrate this process improves the performances of visual classification tasks (e.g. MNIST) in both a rate and spiking networks. Finally, we measure the entropic and energetic effects of sleep, that can be applied to experimental data to verify our theoretical predictions.

METHODS

We modelled a thalamo-cortical system with a two-layer network (the thalamus layer where the input is encoded and a cortical layer, reciprocally connected)l and defined a sleep-inspired activity that reshapes the structure of both synapses and stored memories (as depicted in Figures 1A and B). We implemented a rate based model of a network completely disconnected from external stimuli and assume that the populations of neurons are capable of sustaining an Up-state, a short (few hundreds of ms) state with a sustained level of activity, a hallmark of cortical activity during deep sleep. When the Up state occurs, other populations are activated, generating and hebbian association. We performed similar experiments and found similar results for a spike-based model (not shown in this document). We also considered the natural scenario in which training and testing examples are not equally represented: each example is associated with a mass value that encodes the strength of the expression of that example in the sleeping dynamics. The probability of the Up-state occurring in a population is chosen proportionally to its mass. Coherently with experimental observation, we implemented a homeostatic effect of sleep that progressively lowers the masses of the examples. Our framework was also capable to account for the effect of plasticity on cortico-cortical recurrent connections during sleep-like dynamics. Finally, we made entropy-based measures to the network status at different sleep stages in two different ways: first a microscopic network state analysis and, second, an approximated macroscopic network state analysis to perform measures to be experimentally verified (Figure 2). We applied this analysis to both a 2-class toy dataset and the more complex MNIST dataset in both rate and spiking simulations (as a refinement of network models described in [3] and [4]).

RESULTS AND DISCUSSION

In this document, we present results obtained for the rate-based model trainedover a 2-class dataset, the Crescent Full Moon dataset. We found analogous results for the spiking model trained on more complex datasets (i.e. MNIST Dataset, not shown). In this work, we found theoretical and experimental evidence that stored memories are reorganized following a density-based clustering: close memories group together (see Figure 1C and D). Specifically, we infer the internal representation of the memories from the synaptic weight distributions:

similar synaptic weight patterns, leading also to similar activation patterns in the cortical layer, are associated with closer internal representations. Then, we compute the separability of these memories by a linear separator since we aim to study and model the intrinsic learning capabilities of the network. The huge advantages of such clustering are: not requiring a number of clusters, finding arbitrarily shaped clusters, independence on the number of elements. This improves the linear separability of memories belonging to different classes improving the accuracy during classification tasks (see Figure 1E). We also show that the presence of heterogeneous masses (this can be biologically interpreted as heterogeneity in population recurrent connectivity) speeds up the separability performances for plastic feed-forward connections and improves the separability for plastic recurrent connections. Finally, we propose entropy-based measures that can be applied to experimental data to verify our theoretical predictions (Figure 2). Specifically, to evaluate the quantity of stored information in the network, we measure the entropy associated to the internal representation of memories (see Figure 2A) through both synaptic weights distribution and output layer activity in retrieval; then, we measure the cross-entropy to evaluate the mutual information of associated to the two classes (see Figure 2B). Finally, we also evaluate the energy used by the network at each sleeping step (see Figure 2C). We show that a reduction in both entropy and energy consumption together with an increase in cross-entropy is associated with an improvement in classification performances (as depicted in Figure 2D).

To sum up, in this work we demonstrate the beneficial effect of association in a deep-sleep like activity over a simple thalamo-cortical network in both rate and spiking simulations.

This opens up for future investigation in expanding this analysis to more complex datasets and other stages of sleep.

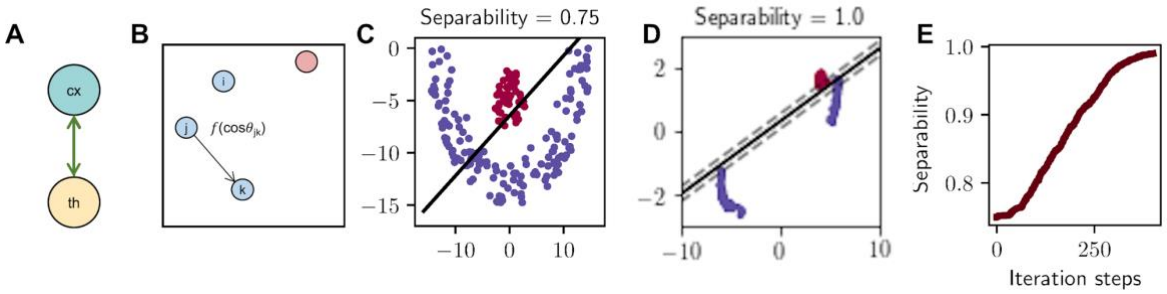

Figure 1: Simulated effects of sleep over stored memories with plastic feedforward connections. A) Network diagram: only thalamo-cortical connections are present. They are plastic during the deep-sleep like activity. B) Graphic representation of the internal "Density-based clustering" dynamics generated by sleep. When the population k produces an Up-state the vectors close to each other are attracted more than further ones and tend to create clusters. C) and D) Internal representation of stored memories at the beginning and the end of the sleep phase respectively. Black solid lines depict the optimal separator identified by the classifier. E) Linear separability of the stored memories as a function of sleeping iterations.

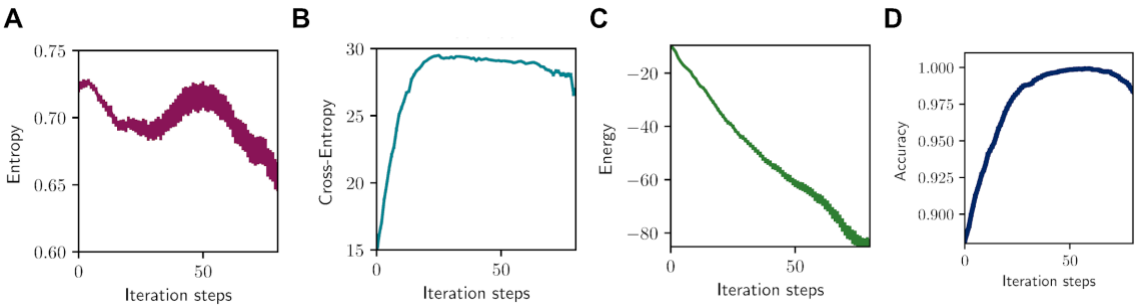

Figure 2: Entropy, cross-entropy and energy measures made over the network status during sleep: an increase in performances is associated with a reduction of entropy and energy consumption and an increase in cross-entropy values. A) Entropy of the system at each sleeping step. B) Cross-entropy between the two classes computed at each iteration of sleep to evaluate the separability of memories. C) Synaptic energy consumption of the network at each iteration step. D) Accuracy of the network in classification at each sleeping step of new unseen examples. It is worth noting that after a given amount of sleep iterations, all the internal representations of memories start to collapse in the same representation, with a consequent reduction in classification performances,

Keywords: deep-sleep, synaptic plasticity, learning

REFERENCES

[1] Walker, M. P. & Stickgold, R. Sleep, memory, and plasticity. Annu. Rev. Psychol. 57, 139–166 (2006).

[2] Jadhav, S. P., Kemere, C., German, P. W. & Frank, L. M. Awake hippocampal sharp-wave ripples support spatial memory. Science 336,1454–1458 (2012).

[3] B. Golosio, C. De Luca, C. Capone, E. Pastorelli, G. Stegel, G. Tiddia, G. De Bonis and P.S. Paolucci "Thalamo-cortical spiking model of incremental learning combining perception, context and NREM-sleep-mediated noise-resilience",2020. arXiv.2003.11859

[4] Capone, C., Pastorelli, E., Golosio, B., Paolucci, P.S. Sleep-like slow oscillations improve visual classification through synaptic homeostasis and memory association in a thalamo-cortical model. Sci Rep 9, 8990 (2019). https://doi.org/10.1038/s41598-019-45525-0

Psychological stress alters cerebellum metabolome

Aikaterini Iliou[1,#], Angeliki-Maria Vlaikou[2,3,#], Markus Nussbaumer[2,3], Dimitra Benaki[1], Emmanuel Mikros[1], Evangelos Gikas[1,4,*], Michaela D. Filiou[2,3,*]

[1] Section of Pharmaceutical Chemistry, Department of Pharmacy, School of Health Sciences, National and Kapodistrian University of Athens (NKUA), Athens, Greece.
[2] Laboratory of Biochemistry, Department of Biological Applications and Technology, School of Health Sciences, University of Ioannina, Ioannina, Greece
[3] Biomedical Research Division, Institute of Molecular Biology and Biotechnology, Foundation for Research and Technology-Hellas (FORTH), Ioannina, Greece
[4] Section of Analytical Chemistry, Department of Chemistry, School of Science, National and Kapodistrian University of Athens (NKUA), Athens, Greece
*mfiliou@uoi.gr , vgikas@chem.uoa.gr
#equal contribution

INTRODUCTION/MOTIVATION

Psychological stress and stress-related conditions constitute a major health challenge in modern societies. Although the brain circuits involved in emotional processing have been intensively studied (1), the involvement of cerebellum in stress responses and the molecular changes induced by stress exposure in this brain region still need to be elucidated. In the last decade, metabolomics has emerged as a powerful tool to investigate the underlying mechanisms of complex diseases, with a plethora of applications in neuropsychiatric and stress-related disorders (2). While alterations of the brain metabolome induced by stress exposure have been observed in hippocampus and other brain regions, stress effects on the cerebellum metabolome are not extensively investigated. Here, we explored the effects of acute stress exposure to the mouse cerebellum metabolome, after exposing mice to an acute stressor using the forced swim test (FST) paradigm.

METHODS

FST was used as an acute stressor in adult male mice. Each mouse was placed into a 2L glass beaker filled with tap water, so that it was impossible to reach the bottom of the beaker or escape and their behavior (time of struggling, swimming, floating and latency to the first floating event) was recorded for 6min. A Nuclear Magnetic Resonance (NMR)-based metabolomics approach was utilized to analyze the metabolomic profiles of the cerebellum between stressed and unstressed mice. A spectral bucketing of 0.001 ppm was applied on the 1D ^{1}H NMR data, which were further normalized to total intensity after removal of water region. The sum of normalized signal (bin) intensities corresponding to each annotated peak was used for relative quantitation of the assigned metabolite (3). Both univariate (parametric and non-parametric) and multivariate (Partial least squares regression-Discriminant analysis, PLS-DA) approaches were implemented, while pathway enrichment analysis of the significant metabolites was performed using Over-Representation Analysis (ORA) in order to highlight the affected biochemical pathways. Finally, we correlated acute stress-induced metabolite alterations and behavioral readouts, using the Spearman's test.

RESULTS AND DISCUSSION

PLS-DA analysis of stressed versus unstressed mice, showed a clear separation between the two groups, indicating that the cerebellum plays a still unexplored role in the pathogenesis of stress (**Figure 1**). In total, 47 known metabolites were annotated in mouse cerebella, 19 of which exhibited significant alterations between stressed and unstressed mice. These include

metabolites related to purine/pyrimidine metabolism, amino acids, neurotransmitters and organic acids. Moreover, aspartate metabolism has emerged as the most prominently affected pathway, followed by the urea cycle, the purine metabolism and the glutamate metabolism. Among others, amino acid neurotransmitters exhibited strong association with FST behavioral parameters (swimming and/or floating).
Overall, our study was able to discriminate stressed from unstressed mice based on the cerebellum metabolome and reported alterations in metabolites mainly implicated in neurotransmission and major metabolic pathways, including energy and purine/pyrimidine metabolism. The present study demonstrates the implication of the cerebellum metabolome to stress responses, highlighting its previously unexplored involvement in stress-related disorders.

Keywords: Forced Swim Test, Cerebellum, Metabolomics, Nuclear Magnetic Resonance, Acute stress, Mouse

Acknowledgements: We thank Dr. Panagiotis Lekkas and the personnel of the University of Ioannina animal facility for expert animal care. This research is co-financed by Greece and the European Union (European Social Fund- ESF) through the Operational Programme «Human Resources Development, Education and Lifelong Learning 2014- 2020» in the context of the project “How mitochondria regulate stress? Let’s ask metabolomics” (MIS 5047652).

REFERENCES

(1) Stressful newborn memories: Pre-conceptual, in utero, and postnatal events. Papadopoulou Z, Vlaikou AM, Theodoridou D, Markopoulos GS, Tsoni K, Agakidou E, Drosou-Agakidou V, Turck CW, Filiou MD, Syrrou M. Front Psychiatry 2019 10:220.

(2) A novel UHPLC-HRMS-based metabolomics strategy enables the discovery of potential neuroactive metabolites in mice plasma, following i.p. administration of the main Crocus sativus L. bioactive component. Karkoula E, Dagla IV, Baira E, Kokras N, Dalla C, Skaltsounis AL, Gikas E, Tsarbopoulos A, J Pharm Biomed Anal 2020 177:112878.

(3) Recommended strategies for spectral processing and post-processing of 1D 1H-NMR data of biofluids with a particular focus on urine. Emwas AH, Saccenti E, Gao X, McKay RT, Dos Santos VAPM, Roy R, Wishart DS, Metabolomics. 2018 14:31.

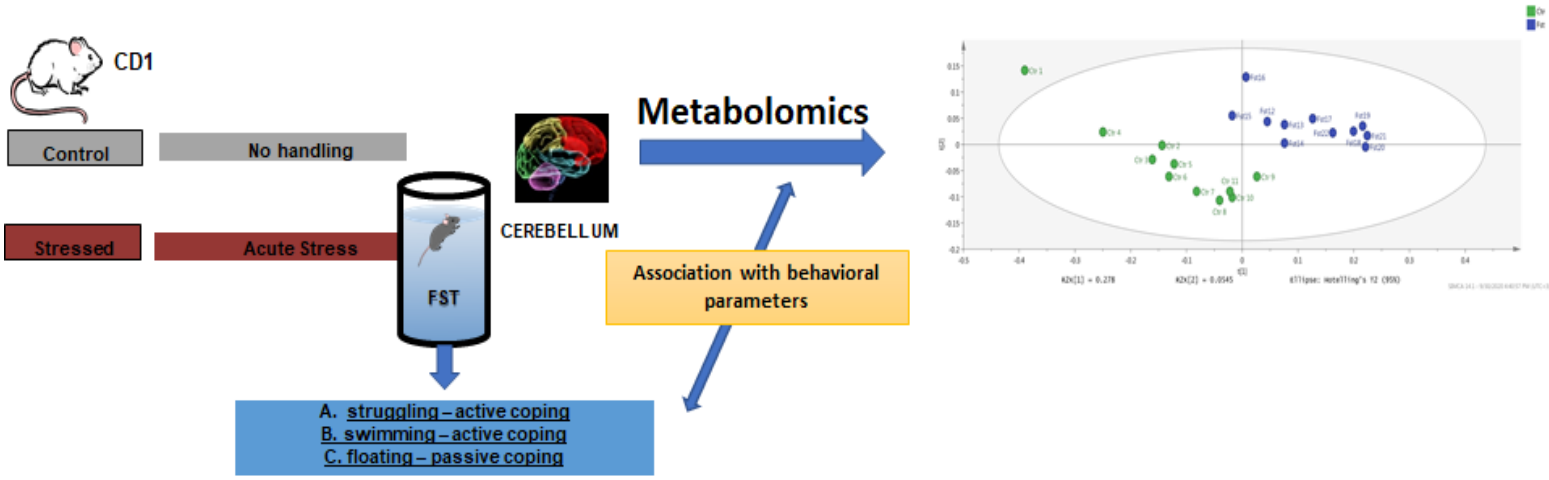

Figure 1: Schematic representation of the experimental workflow. Mice were subjected to FST acute stress, while unstressed mice were used as controls. Comparative ^{1}H 1D NMR metabolomics analysis was performed in mouse cerebellum. Principal Component (PC) scores plot from PLS-DA model of 1D ^{1}H NMR metabolomics data from the stressed (blue) versus control (green) group showed clear discrimination of the two groups, highlighting a role of cerebellum metabolome in stress response. Altered pathways between the stressed and control groups were identified and selected metabolites were further correlated with FST behavioral parameters.

Dynamics of hippocampal activity patterns during spatial learning

Mengmeng Li[1,2], Jiantao Fan[1,2], Shuguan Cheng[1,2], Zhigang Shang[1,2]*, Hong Wan[1,2*]

[1] School of Electrical Engineering, Zhengzhou University, Zhengzhou, China
[2] Henan Key Laboratory of Brain Science and Brain-Computer Interface Technology, Zhengzhou, China
*zhigang_shang@zzu.edu.cn, wanhong@zzu.edu.cn

INTRODUCTION/MOTIVATION

The hippocampus (Hp) has been proved to be mainly related to spatial learning [1]. Hippocampal neurons are highly adaptive to process and encode the spatial-related information, indicating the crucial role of Hp for spatial learning [2]. Previous studies have shown that the avian Hp is functionally homologous with the mammals [3], which plays an important role in path planning and adjustment of spatial learning process [4][5]. However, the dynamics of hippocampal activity patterns during spatial learning is still unclear. In this study, we explored the neural response patterns of the pigeon recorded from Hp during a goal-directed spatial learning task.

METHODS

In our experiments, the pigeons were trained to carry out a goal-directed spatial learning task in a maze, as shown in Figure 1. At the beginning of the trial, the hamper was opened to provide food at the goal location, and the pigeons were trained to learn a preferred path to the goal. If the pigeon arrived at the goal, this trial was recorded as a correct one. After enjoying the food reward provided in the food hampers, they were trained to go back to the starting position to start the next trial. When a pigeon could reliably perform the trial through a preferred path, in which more than 80% of the total trail numbers were corresponding to the same one path on two consecutive days, it was considered that the pigeon finished the learning task. The infrared detectors distributed on all of the pathlets along the paths were used to define the beginning time and end time for signal segmentation. The behavioral data of the pigeons were recorded by the observation camera placed on the ceiling during spatial learning, to calculate the behavioral response accuracy and obtain the time the pigeons spent from the starting position to the goal. Local field potential (LFP) signals in the Hp of the pigeons were acquired and preprocessed. Power spectral density (PSD) analysis, time-frequency (TF) analysis based on wavelet transform, and functional network (FN) analysis based on coherence coefficient were carried out to explore the temporal dynamics of neural patterns during spatial learning.

RESULTS AND DISCUSSION

For all of the sessions from five pigeons, the behavioral correct rate and the average time the pigeons spent from the starting position to the goal under different learning stages were calculated. The results are shown in Figure 2 (A) and (B). The results reveal that the total duration from the starting position to the goal gradually decreases along with the improvement of the behavioral correct rate. To explore the neural activity dynamic patterns during spatial learning further, we calculated the coherence coefficients of the LFPs between all channels in Hp and visualized the corresponding binarized FNs in the theta band during different learning stages, which are shown in Figure 2 (C). It can be seen that the functional connection in Hp becomes denser along with spatial learning. It suggests that the spatial

learning process modulates the dynamic network connection pattern in Hp. For further quantitative analysis, the topological characteristics of FN including clustering coefficient and global efficiency are analyzed, and the results are shown in Figure 2 (D) and (E). Both of these two topological characteristic parameters show a rising trend along with the advancement of the learning process.

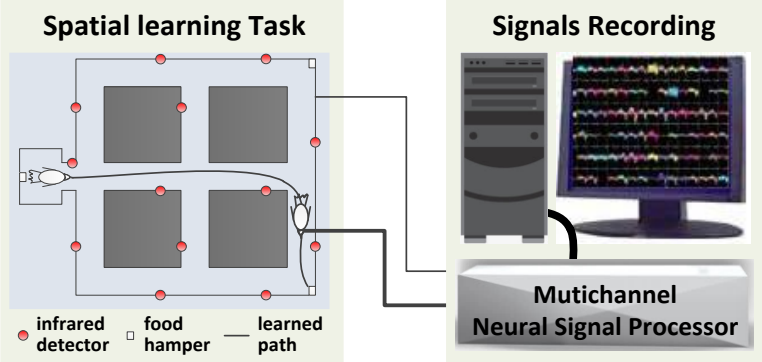

Figure 1. Diagram of the maze apparatus for pigeons and experiment procedures.

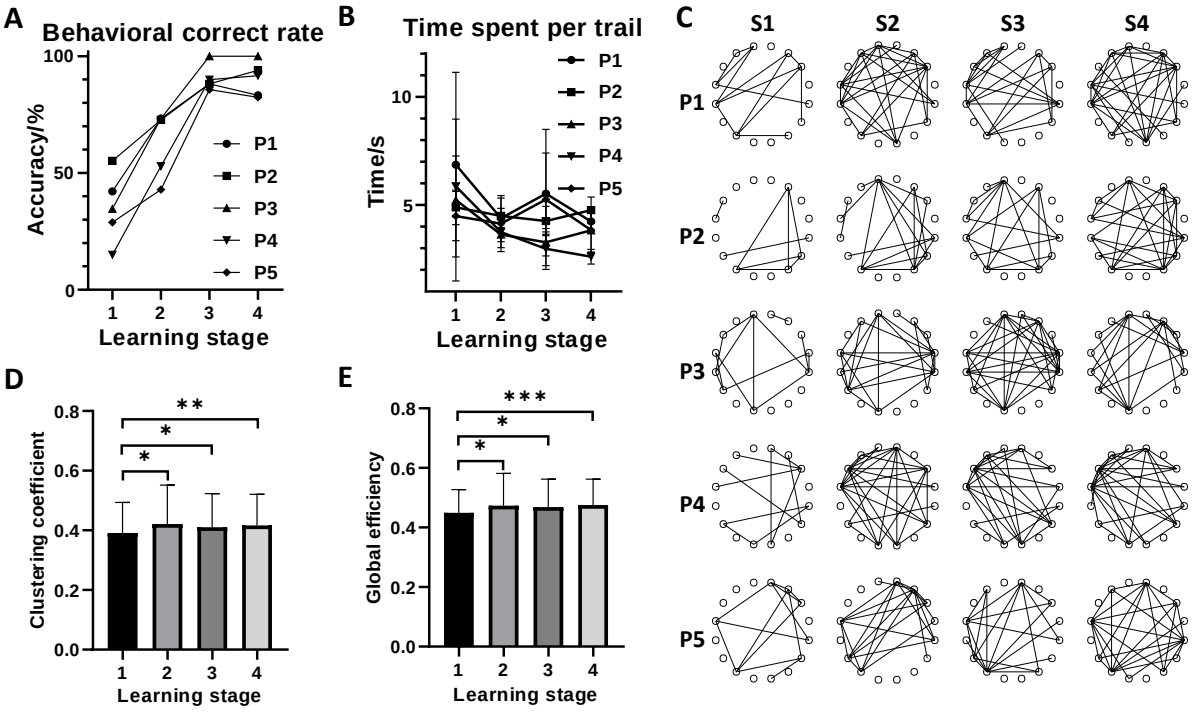

Figure 2: Dynamics of behavioral data and hippocampal activity patterns during spatial learning of five pigeons. (A) behavioral response accuracy, (B) time spent from the starting position to the goal, (C) binarized FNs, in which each hollow circle indicates a channel, (D) topological characteristic clustering coefficient of FN (mean of all pigeons), (E) topological characteristic global efficiency of FN (mean of all pigeons). Statistically significant were indicated by p value as follows: $*: p < 0.05$, $**: p < 0.01$, $***: p < 0.001$.

This current study focuses on the Hp of the pigeon, which is the most concerned target brain region in the study of spatial learning mechanism and explored the dynamics of hippocampal activity patterns during spatial learning. We can conclude that the spatial learning process modulates the dynamic neural pattern of Hp. The dynamic changes of brain network connectivity in Hp during spatial learning may contribute to the understanding of the potential mechanism of spatial cognition. On the other hand, Hp is not the solely responsible region for complex spatial processing independently. Is there any similar or different phenomenon in other spatial-related regions, and the dynamic neural connection patterns between the regions contained in a wider local network remain to be further analyzed and explored.

Keywords: dynamics, hippocampus, spatial learning, pigeon

REFERENCES

[1] Ólafsdóttir HF, Bush D, Barry C (2018). The role of hippocampal replay in memory and planning. Current Biology 28: R37-R50.
[2] O'Keefe J, Nadel LM (1978). The hippocampus as a cognitive map. Clarendon Press, Oxford.
[3] Herold C, Schloemer P, Mafoppa-Fomat I et al. (2019). The hippocampus of birds in a view of evolutionary connectomics. Cortex 118: 165-187.
[4] Kahn MC, Bingman VP (2009). Avian hippocampal role in space and content memory. European Journal of Neuroscience 30: 1900-1908.
[5] Mouritsen H, Heyers D, Güntürkün O (2016). The neural basis of long-distance navigation in birds. Annual Review of Physiology 78: 133-154.

Behavioural characteristics of perceptual inference in a multimodal associative learning paradigm

Zsófia Pálffy[1]*, Kinga Farkas[1,2]**, Gábor Csukly[2], Bertalan Polner[1]***

[1] Department of Cognitive Science, Budapest University of Technology and Economics, Budapest, Hungary
[2] Department of Psychiatry and Psychotherapy, Semmelweis University, Budapest, Hungary
*zsofiapalffy@edu.bme.hu
**farkas.kinga@edu.bme.hu
***bpolner@cogsci.bme.hu

INTRODUCTION/MOTIVATION

The Bayesian brain theory states that during perception the brain performs inference when it combines sensory information with prior expectations, all being weighted by their uncertainty [1]. It has been shown that priors influencing perception of ambiguous stimuli can be shaped with associative learning [2]. However, the differential effect of auditory vs. visual associative cues on visual motion perception is still to be investigated. Furthermore, the test-retest reliabilities of variables derived from behavioural tasks are highly variable in the literature [3], and evaluation of these appears especially underrepresented in contemporary perceptual inference research.

METHODS

We measured healthy individuals' (N=29; 14 men, mean[SD] age = 26.6[5.5] years) performance on a perceptual inference task twice with a one-week delay (640 trials each). They indicated the perceived direction of illusory motion of dot pairs (see Figure 1A). A visuo-acoustic cue preceded the target stimulus and probabilistically predicted the direction of the motion. In 30% of the trials, motion direction was ambiguous, and in half of these trials, the auditory and the visual dimension of the cue predicted opposing directions (see Figure 1B). Cue-stimulus contingency could change every 40 trials.

RESULTS AND DISCUSSION

Slower responses to less predictable, relative to more predictable non-ambiguous stimuli and the increased rate of cue-congruent decisions on ambiguous trials showed the impact of associative learning on perceptual decisions. Importantly, on ambiguous trials participants made more decisions congruent with the prediction of the acoustic dimension, when the visual and the auditory dimensions of the cue predicted conflicting directions of motion. Furthermore, all the above effects had substantial inter-individual variability which showed high test-retest reliability ($r_s > 0.6$, see Figure 2).

Overall, priors based on auditory information seem to have a stronger weight during the perception of illusory visual motion, although the data suggests large differences in perceptual learning and/or decision making. Whether the characteristics of visual vs. auditory processing, attentional processes or encoding the uncertainty of the visual modality caused these behavioural effects, is still up to discussion. Beyond follow-up behavioural experiments, computational modelling combined with neuroimaging could allow testing further hypotheses regarding the potential mechanisms.

Keywords: perceptual inference, Bayesian brain theory, test-retest reliability

Acknowledgements: B.Polner's work was funded by BME Biotechnology Project (FIKP-BIO) and NKFI/OTKA K 12859.

REFERENCES

[1] Friston, K. (2010). The free-energy principle: A unified brain theory? *Nature Reviews Neuroscience*, *11*(2), 127–138. https://doi.org/10.1038/nrn2787

[2] Weilnhammer, V. A., Stuke, H., Sterzer, P., & Schmack, K. (2018). The Neural Correlates of Hierarchical Predictions for Perceptual Decisions. Journal of Neuroscience, 38(21), 5008–5021. https://doi.org/10.1523/JNEUROSCI.2901-17.2018

[3] Enkavi, A. Z., Eisenberg, I. W., Bissett, P. G., Mazza, G. L., MacKinnon, D. P., Marsch, L. A., & Poldrack, R. A. (2019). Large-scale analysis of test–retest reliabilities of self-regulation measures. Proceedings of the National Academy of Sciences, 116(12), 5472-5477.

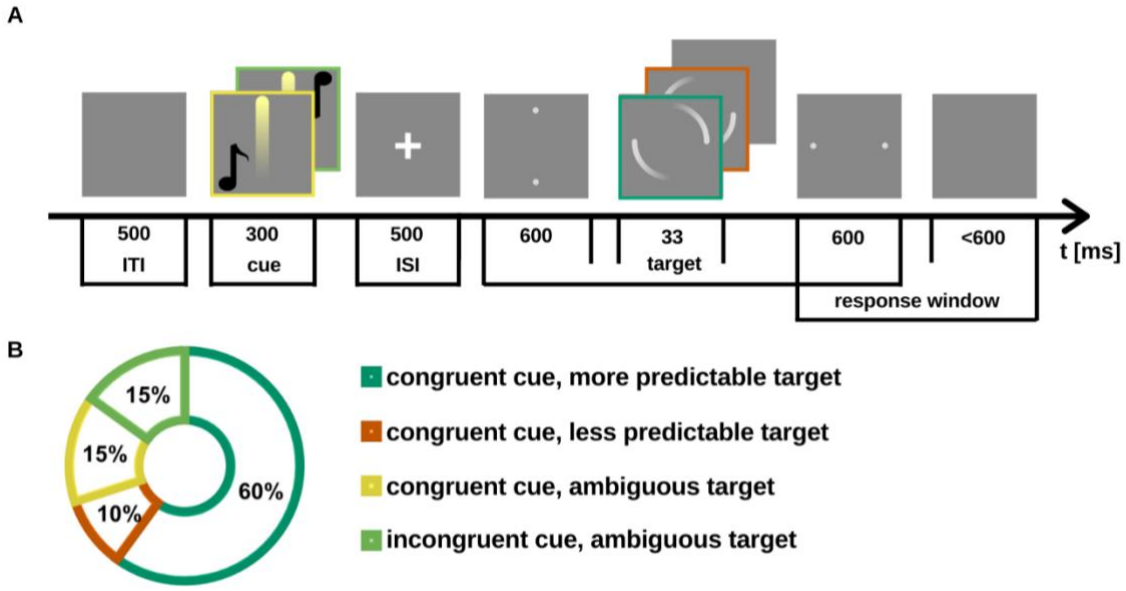

Figure 12 Experimental design (A) and distribution of conditions in every 40 trials (B). Conditions differ in the availability of sensory information, which affects the likelihood: on unambiguous trials a motion illusion sets the likelihood probability of the showed tilt close to 1, whereas on ambiguous trials there is no motion illusion, setting the likelihood probability of each tilt close to 0.5. Since most trials follow a rule, after the cues were presented, the prior probability of the direction it is associated with increases. But unambiguous trials differ in regularity, and it affects the confidence in the learnt priors: more predictable targets are expected from the priors, they increase the precision, whereas less predictable targets are unexpected, they decrease the precision. As their mind unconsciously infers the posterior probability of each direction, they indicate the perceived direction which was the most probable. We hypothesise that reaction time indicates confidence (posterior probability extremely above chance level).

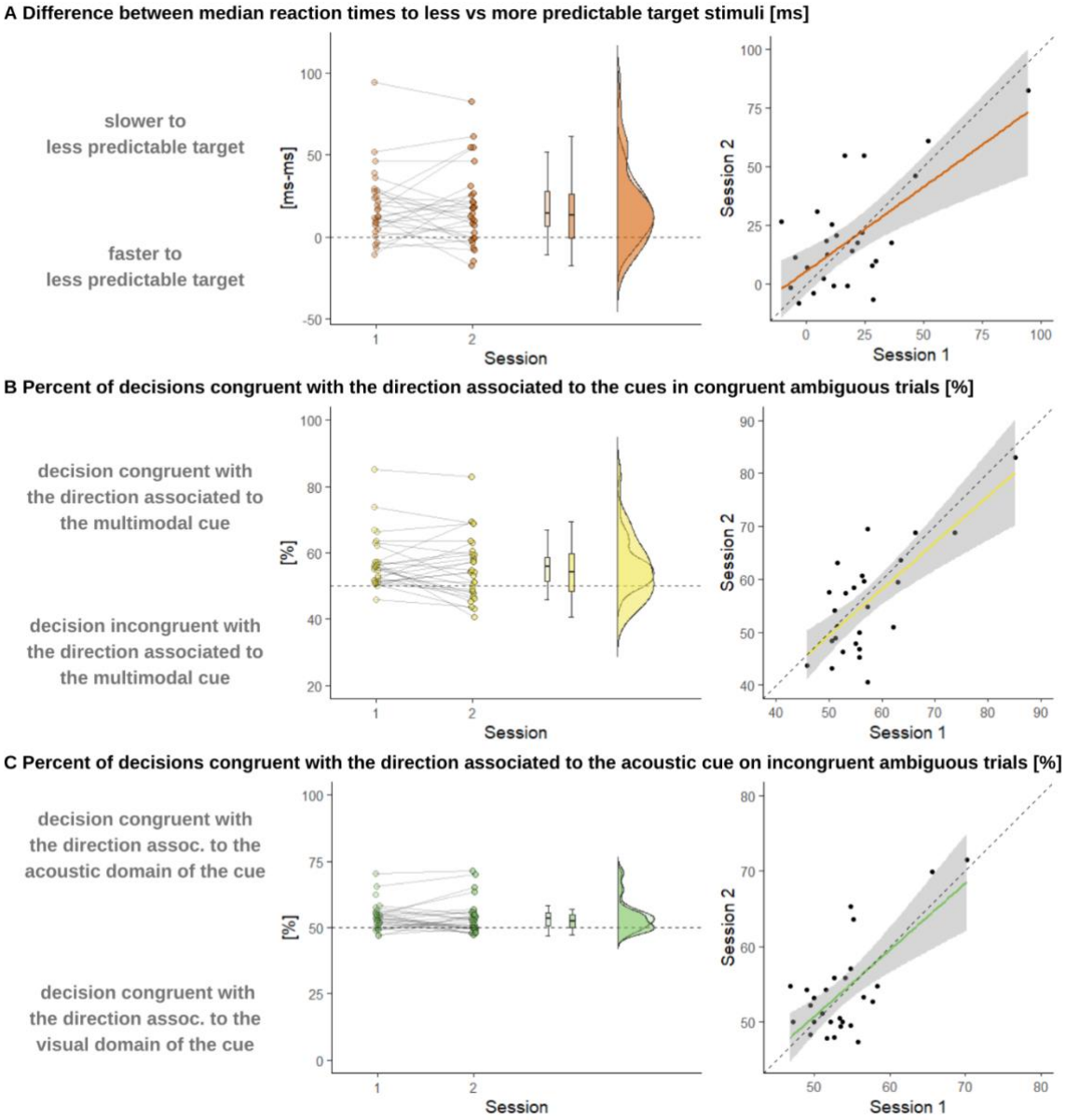

Figure 13 Behavioural results. [left] On the left, each dot represents a participant, values from each session connected along the x axis, a boxplot (median, 50% CI) is shown in the middle, and the distribution for each session can be seen on the right. [right] Each dot represents a participant's performance in session 1 and 2 on the x and the y axis, respectively. Trend line shows linear fit with 95% confidence interval and the dashed line indicates the hypothetical perfect correlation. [A] Slowing down to unexpected tilts. On the y axis, median reaction times differences are presented when cues were followed by less vs more predictable tilting illusion. If there was no difference between these conditions, dots were mostly around 0 ms (level shown with dashed line). Test-retest stability was high. [B] Bias towards direction associated with cue. Along the y axis, we present the percent of decisions congruent with the direction associated with the cues under ambiguity and after congruent cues. Associative learning influenced perceptual inference, as participants made more perceptual decisions consistent with the associative cues (above-chance level [50% shown with dashed line]). [C] Bias towards direction associated with tone. Along the y axis, we present the percent of decisions consistent with the direction associated with the acoustic cue in ambiguity after incongruent cues (where the acoustic and visual cues were associated with different directions). Auditory-visual associative learning slightly dominantly influenced perceptual inference, as participants made more perceptual decisions consistent with the auditory cue (above-chance level [50% shown with dashed line]).